HHS Public Access

Author manuscript

Sci Immunol. Author manuscript; available in PMC 2024 May 15.

Published in final edited form as:

Sci Immunol. 2024 February 16; 9(92): eadj7029. doi:10.1126/sciimmunol.adj7029.

T cell help shapes B cell tolerance

Elliot H. Akama-Garren[1,2], **Xihui Yin**[3], **Tyler R. Prestwood**[3], **Minghe Ma**[1], **Paul J. Utz**[3], **Michael C. Carroll**[1,*]

[1]Program in Cellular and Molecular Medicine, Boston Children's Hospital, Harvard Medical School, Boston, MA 02115, USA.

[2]Harvard-MIT Health Sciences and Technology, Harvard Medical School, Boston, MA 02115, USA.

[3]Department of Medicine, Stanford University School of Medicine, Stanford, CA 94305, USA.

Abstract

T cell help is a crucial component of the normal humoral immune response, yet whether it promotes or restrains autoreactive B cell responses remains unclear. Here, we observe that autoreactive germinal centers require T cell help for their formation and persistence. Using retrogenic chimeras transduced with candidate TCRs, we demonstrate that a follicular T cell repertoire restricted to a single autoreactive TCR, but not a foreign antigen–specific TCR, is sufficient to initiate autoreactive germinal centers. Follicular T cell specificity influences the breadth of epitope spreading by regulating wild-type B cell entry into autoreactive germinal centers. These results demonstrate that TCR-dependent T cell help can promote loss of B cell tolerance and that epitope spreading is determined by TCR specificity.

INTRODUCTION

T cell help to B cells is a fundamental component of the adaptive immune system. Signals from follicular T cells to germinal center (GC) B cells facilitate somatic hypermutation, class switch recombination, affinity maturation, and memory B cell formation. Peripheral B cell tolerance is maintained in the GC through mechanisms such as clonal redemption and clonal anergy (1–7), but failures in these mechanisms can lead to production of pathogenic, class-switched, and epitope-spread autoantibodies (8–10). Although the function of follicular T cells, including T follicular helper (T_{FH}) and T follicular regulatory (T_{FR}) cells, has been well characterized in the normal GC (11, 12), the role of these cells in the autoreactive GC is less well understood (13–15).

Alterations in follicular T cell frequency and phenotype in autoantibody-mediated disease suggest that T cell help is critical for regulating B cell tolerance. T_{FH} and T_{FR} frequencies

*Corresponding author. michael.carroll@childrens.harvard.edu.

Author contributions: Conceptualization: E.H.A.-G. and M.C.C. Methodology: E.H.A.-G. and T.R.P. Investigation: E.H.A.-G., X.Y., and M.M. Visualization: E.H.A.-G. Funding acquisition: E.H.A.-G., P.J.U., and M.C.C. Project administration: P.J.U. and M.C.C. Supervision: P.J.U. and M.C.C. Writing (original draft): E.H.A.-G. Writing (review and editing): E.H.A.-G. and M.C.C.

Competing interests: The authors declare that they have no competing interests.

are disrupted in systemic lupus erythematosus, myasthenia gravis, Sjögren's syndrome, multiple sclerosis, autoimmune thyroid disease, and rheumatoid arthritis (16–31). Systemic autoimmunity in *Roquin*$^{san/san}$ mice is T cell dependent (32), likely because Roquin-1 targets key T_{FH} genes, such as *Icos* and *Ox40* (33–35). Advances in single-cell T cell receptor sequencing (scTCR-seq) have allowed for interrogation of the follicular T cell repertoire, revealing that T_{FH} and T_{FR} cells have nonoverlapping repertoires that expand but do not develop clonality in response to immunization with foreign antigens (36–38).

We hypothesized that despite widespread bystander activation, a subset of follicular TCR clones can provide T cell help to break B cell tolerance. To determine the role of T cell help and TCR specificity in autoreactive GCs, we developed follicular T cell–deficient mouse models of autoantibody disease. These models revealed that follicular T cells are necessary for the formation and persistence of spontaneous autoreactive GCs. We found that among a pool of polyclonal follicular T cells, a subset of autoimmune-enriched specificities can recognize autoantigen. Furthermore, these autoreactive TCRs, but not a model TCR, are sufficient to rescue spontaneous GC formation, facilitate wild-type (WT) B cell entry to autoreactive GCs, and direct epitope spreading toward specific autoantigens.

RESULTS

Autoreactive GC formation and persistence is T cell dependent

We tested T cell dependency in mice using the *Icos*$^{-/-}$ and *SAP*$^{-/-}$ models of follicular T cell deficiency (39, 40). To confirm the necessity of inducible T-cell costimulator (ICOS) and SLAM-associated protein (SAP) for provision of T cell help, we studied primary GC responses against foreign antigens using immunization with 4-hydroxy-3-nitrophenylacetyl hapten conjugated to ovalbumin (NP-OVA) or sheep red blood cells and chronic GC responses against commensal bacterial antigens using the mesenteric lymph node. ICOS- and SAP-deficient mice had decreased follicular T cell frequency and a corresponding loss of GC B cells and antibody-secreting cells (ASCs) (fig. S1, A to F), confirming that GC formation and ASC output are dependent on T cell help mediated by ICOS or SAP. Follicular T cell formation was less dependent on SAP than ICOS (fig. S1B), consistent with previous reports that early CD4 priming and T_{FH} differentiation are ICOS dependent but SAP independent (41–43). Chronic spontaneous GCs in the mesenteric lymph node were also less dependent on SAP than ICOS (fig. S1D), similar to recent observations in Peyer's patches (44).

Given the T cell dependence of primary B cell responses against foreign antigens, we next asked whether autoreactive GCs similarly require T cell help. To test the necessity of T cell help for autoreactive GC formation, we crossed 564Igi mice (45), which have heavy- and light-chain knockins of an autoreactive B cell receptor against ribonuclear complexes (46), onto ICOS- or SAP-deficient backgrounds. As expected, ICOS- and SAP-deficient mice lacked follicular T cells with near complete absence of T_{FH} ($CD4^+CXCR5^+PD1^+ICOS^+FoxP3^-$) and TFR ($CD4^+CXCR5^+PD1^+ICOS^+FoxP3^+$) cells (Fig. 1, A and B). 564Igi;*Icos*$^{-/-}$ and 564Igi;*SAP*$^{-/-}$ mice also failed to form GCs, class-switched immunoglobulin G1 (IgG1), and age-associated B cells (ABCs; $CD11c^+CD21/35^-B220^+CD138^-GL7^-CD38^+IgD^-$) (Fig. 1, C and D), suggesting that T

cell help is necessary for both autoreactive GC formation and early GC-extrinsic B cell activation. 564Igi;$Icos^{-/-}$ and 564Igi;$SAP^{-/-}$ spleens had decreased GC frequency despite presence of follicular dendritic cells (FDCs) and follicular architecture (Fig. 1, E and F). ASCs were less proliferative in both 564Igi;$Icos^{-/-}$ and 564Igi;$SAP^{-/-}$ mice (Fig. 1G), but only 564Igi;$Icos^{-/-}$ mice had decreased ASC formation (Fig. 1H). Persistence of autoreactive ASCs suggests that although T cell help is necessary for ASC proliferation, autoimmune mice have an ICOS-dependent but SAP-independent source of ASCs. Antinuclear antibody (ANA) testing of 564Igi sera demonstrated nucleolar and cytoplasmic staining (Fig. 1I), likely representing autoreactivity against multiple autoantigens. Functional autoantibody production was decreased in 564Igi;$Icos^{-/-}$ and 564Igi;$SAP^{-/-}$ mice, resulting in decreased ANA staining (Fig. 1I) and glomerular autoantibody deposition (Fig. 1J). These results suggest that as in foreign antigen–elicited GCs, initiation of autoreactive GCs and autoantibody production require T cell help.

We next asked whether T cell help is necessary for not only the formation but also the persistence of chronic autoreactive GCs. To establish a model of inducible loss of T cell help, we crossed $Cd4^{CreERT2}$ mice onto the $Bcl6^{fl/fl}$ background to generate mice in which delivery of tamoxifen leads to inducible deletion of the follicular T cell lineage–defining transcription factor B cell lymphoma 6 (Bcl6) (47). We confirmed that $Cd4^{CreERT2}$;$Bcl6^{fl/fl}$ mice have inducible loss of T_{FH}, T_{FR}, and GC B cell responses to primary immunization with foreign antigen (fig. S2). To test the necessity of continuous T cell help in chronic autoreactive GCs, we crossed $Cd4^{CreERT2}$;$Bcl6^{fl/fl}$ mice onto the 564Igi background. Bcl6 deletion led to inducible loss of T_{FH}, T_{FR}, and GC responses in autoimmune mice (fig. S3, A to E), suggesting that T cell help is necessary for the persistence of autoreactive GCs. However, Bcl6 deletion did not alter ABC or ASC frequency or ASC proliferation in autoimmune mice (fig. S3, E and F), suggesting that loss of T cell help does not immediately affect early GC-extrinsic B cell activation or ASC presence. Although Bcl6 depletion led to loss of splenic GCs (fig. S3G), it did not alter ANA reactivity (fig. S3H), likely due to the extended half-life of serum autoantibodies. These results suggest that in addition to their initiation, persistence of autoreactive GCs requires continuous T cell help.

Follicular T cell repertoires are polyclonal and dynamic

Given the necessity of T cell help for autoreactive GC formation and persistence, we next asked whether follicular T cell–driven loss of B cell tolerance is due to a clonal follicular T cell response. To visualize T cell clonality in situ, we crossed $Cd4^{CreERT2}$ mice onto the $R26^{con/con}$ background to generate mice in which delivery of tamoxifen leads to inducible labeling of CD4 T cells with 1 of 10 randomly generated confetti color combinations (48). We first tested our ability to visualize follicular T cell clonality in foreign antigen–elicited GCs by treating $Cd4^{CreERT2}$;$R26^{con/con}$ mice with tamoxifen, followed by primary immunization with NP-conjugated to chicken gamma globulin (NP-CGG) and analysis of the draining inguinal lymph node up to 30 days after immunization (fig. S4A). Labeled follicular T cells were observable as early as 3 days after immunization (fig. S4B). However, in contrast to GC B cells (49), follicular T cells remained polyclonal up to 30 days after labeling (fig. S4B). These results suggest that in contrast to GC B cells, follicular T cells

in foreign antigen–elicited GCs remain polyclonal over the course of the primary immune response.

To assess the clonality of follicular T cells in chronic autoimmune GCs in situ, we generated mixed bone marrow chimeras in which irradiated *Icos*$^{-/-}$ mice were reconstituted with 564Igi;*Icos*$^{-/-}$ and *Cd4*^{CreERT2};*R26*$^{con/con}$ bone marrow. In this model, follicular T cells should only originate from *Cd4*^{CreERT2};*R26*$^{con/con}$ bone marrow. Six weeks after reconstitution, autoimmune bone marrow chimeras were treated with tamoxifen, left for 5 weeks to establish clonality, administered phycoerythrin (PE) anti-CD21/35 to label FDCs, and analyzed by intravital multiphoton microscopy (Fig. 2A). Similar to foreign antigen–elicited GCs, chronic autoimmune GCs had highly polyclonal follicular T cells (Fig. 2, B and C, and movie S1). Individual GCs and even distinct regions of the FDC network harbored a multitude of follicular T cell clones (movie S1), suggesting that a breadth of T_{FH} and T_{FR} TCR specificities are present in a single GC. Intravital multiphoton microscopy also allowed for tracking of individual follicular T cell clones over time. We observed both the exit and entry of follicular T cell clones of different confetti origins in an individual GC over a span of 10 to 15 min (Fig. 2D and movie S2), suggesting that follicular T cells in autoimmune GCs are both polyclonal and dynamic.

We also assessed follicular T cell clonality in autoimmune GCs by reanalyzing single-c ell RNA sequencing (scRNA-seq) and scTCR-seq of follicular T cells from autoimmune bone marrow chimera spleens 10 weeks after reconstitution (Fig. 3A) (50). Follicular T cells from both immunized and autoimmune bone marrow chimeras exhibited a similar degree of clonal expansion (Fig. 3B) and were not distinguishable by T cell repertoire similarity scores (TRSSs) (Fig. 3C). However, unweighted network analysis separated immunized and autoimmune follicular T cell repertoires on the basis of sharing of expanded CDR3β clones between mice (Fig. 3D), suggesting that there is an intrinsic difference in the immunized and autoimmune follicular T cell repertoires when clonal expansion and overlap are considered.

To compare the clonality of subsets of follicular T cells, we mapped the TCR repertoire onto the transcriptional landscape using paired scRNA-seq and scTCR-seq datasets. Unsupervised clustering identified eight clusters of follicular T cells, most prominently T_{FR} and sclerostin domain containing 1 (Sostdc1) T_{FH} cells, which were decreased and increased, respectively, in autoimmune bone marrow chimeras (fig. S5, A to C). The follicular T cell subsets were clonally and transcriptionally distinct, with limited clonotype sharing between clusters (fig. S5, D and E). Differential gene expression analysis revealed that each cluster was also transcriptionally distinct in autoimmune bone marrow chimeras (fig. S5F), with notable increases in *Ly6a*, *Def8*, and *Cmss1* in almost all subsets. Although different follicular T cell clusters had varying degrees of clonality, most clusters exhibited a similar degree of clonal expansion in immunized and autoimmune bone marrow chimeras (fig. S5G), suggesting that follicular T cell subset, but not GC type, influences follicular T cell clonality. These observations suggest that although follicular T cells are transcriptionally distinct in autoimmune bone marrow chimeras, follicular T cell subsets are similarly polyclonal in both immunized and autoimmune GCs. This condition-agnostic polyclonality is consistent with our in situ observations of a multi–confetti color follicular T cell response in both foreign antigen–elicited and autoimmune GCs.

To ask whether follicular T cell–dependent loss of B cell tolerance is due to an antigen-specific group of TCRs, we applied four orthogonal methods of in silico prediction of TCR specificity to compare the immunized and autoimmune follicular T cell repertoires. Grouping of lymphocyte interactions by paratope hotspots (GLIPH2) revealed an unexpected degree of shared specificity group expansion between immunized and autoimmune follicular T cell repertoires (Fig. 3, E and F), suggesting that many follicular T cells can recognize similar antigens independent of GC type. Similarly, Geometric Isometry–based TCR Alignment Algorithm (GIANA4), TCRdist3, and DeepTCR2 dimensionality reduction were unable to separate immunized from autoimmune follicular T cell repertoires (Fig. 3G), confirming that they likely share predicted specificities. Repertoire-wide pairwise comparisons of TCRdist3 scores identified clusters of closely related TCRs between immunized and autoimmune bone marrow chimeras (Fig. 3H), indicating that follicular T cells from immunized and autoimmune GCs are similar and might recognize the same antigens.

Although in silico prediction of TCR specificity revealed a high degree of shared predicted antigen reactivities in the immunized and autoimmune follicular T cell repertoires, there was a minority of specificity groups that exhibited preferential expansion in either immunized or autoimmune bone marrow chimeras (Fig. 3, E and G), consistent with our ability to separate immunized from autoimmune follicular T cell repertoires when accounting for CDR3β sharing and expansion (Fig. 3D). Computational prediction of TCR autoreactivity using CDR3βmr-specific TCR-intrinsic regulatory potential (mTiRP) (51) revealed inversion of mTiRP scores between immunized and autoimmune repertoires in Sostdc1 and effector-like T_{FH} cells (Fig. 3I), suggesting that Sostdc1 T_{FH} cells might be less autoreactive, whereas effector-like T_{FH} cells might be more autoreactive in autoimmune chimeras. These changes potentially represent disparate fates of autoreactive versus nonautoreactive T_{FH} cells in autoimmune bone marrow chimeras (51), although in silico repertoire analyses require in vivo validation. Together, these results suggest that although most of the follicular T cell repertoire represents lowly expanded TCRs capable of binding a pool of condition-agnostic antigens, a minority of the repertoire that is capable of binding to a distinct set of antigens expands in autoimmune GCs. We hypothesized that this set of TCRs is responsible for the T cell dependence of autoreactive GCs.

Follicular T cell initiation of autoreactive GCs is TCR dependent

We next asked whether loss of B cell tolerance is determined by TCR specificity. To establish mice with a TCR-restricted follicular T cell repertoire, we generated mixed bone marrow chimeras in which irradiated *Icos*$^{-/-}$;CD45.1 mice were reconstituted with 564Igi;*Icos*$^{-/-}$ bone marrow mixed with B6;CD45.1, *Icos*$^{-/-}$;CD45.1, or OTII;CD45.1 bone marrow (Fig. 4A). In this model, autoimmune bone marrow chimeras with B6 bone marrow (BM.564.B6) have a complete WT follicular T cell repertoire, autoimmune bone marrow chimeras with *Icos*$^{-/-}$ bone marrow (BM.564.ICOS) lack any follicular T cells, and autoimmune bone marrow chimeras with OTII bone marrow (BM.564.OTII) have follicular T cells with a restricted TCR repertoire against OVA. In addition, CD45.1 may be used as a congenic marker to distinguish hematopoietic cells of non-564Igi (autoimmune) origin.

Twelve weeks after reconstitution, BM.564.ICOS mice lacked follicular T cells (Fig. 4, B and C). Follicular T cell presence was rescued by the inclusion of WT bone marrow but not OTII bone marrow (Fig. 4, B to D). Analysis of CD4 subsets revealed an increase in naïve $CD44^{-}CD62L^{+}$ cells with a corresponding decrease in $CD44^{+}PD1^{+}$-activated cells in BM.564.ICOS and BM.564.OTII mice (Fig. 4, E and F), supporting a global decrease in CD4 activation in autoimmune chimeras lacking T cell help or with only T cell help toward OVA. CD4 cells also had decreased $FoxP3^{+}$ regulatory T cells (T_{regs}) in BM.564.ICOS and BM.564.OTII mice (Fig. 4G), consistent with prior reports of ICOS-mediated control of the homeostatic T_{reg} pool (52). Extrafollicular (EFO) CD4 T cell frequency, programmed cell death protein 1 (PD1), and CD44 expression were also decreased in BM.564.ICOS and BM.564.OTII mice (Fig. 4, H to J), suggesting that the presence and activation of EFO CD4 T cells are TCR dependent in B cell–driven autoimmune disease. These findings illustrate the inability of a restricted OTII follicular T cell repertoire to overcome CD4 T cell phenotypic changes due to ICOS deficiency in B cell–driven autoimmune disease.

Given these CD4 T cell deficiencies, we next asked whether a restricted follicular T cell repertoire was sufficient to rescue spontaneous autoimmune GC formation. BM.564.ICOS mice failed to form spontaneous autoimmune GCs or ASCs, both of which were rescued with a WT follicular T cell repertoire but not an OTII-restricted repertoire (Fig. 4, K and L), indicating that loss of B cell tolerance is TCR dependent. Enrichment of non-5 64Igi–derived B cells in the GC may be a precursor to epitope spreading (45) that can be quantified by calculating the ratio of CD45.1 frequency in the GC compartment to the CD45.1 frequency in the follicular B cell compartment. BM.564.B6 GCs were largely populated by CD45.1 cells (Fig. 4M), consistent with previous observations of WT B cell entry into and dominance of spontaneous autoimmune GCs (45). BM.564. ICOS and BM.564.OTII mice exhibited decreased CD45.1 enrichment in the GC (Fig. 4M), suggesting that epitope spreading represented by WT B cell entry into autoreactive GCs is rescued with a WT follicular T cell repertoire but not fully with an OTII-restricted repertoire. Both GC B cells and ASCs expressed decreased Ki67 in BM.564.ICOS and BM.564.OTII mice (Fig. 4N), indicating that GC B cell and ASC proliferation can be rescued by a WT but not a restricted OTII follicular T cell repertoire in autoimmune bone marrow chimeras. Notably, B cells increased expression of ICOSL in BM.564.ICOS and BM.564.OTII mice (Fig. 4O), likely representing a homeostatic response to loss of CD4 T cell–derived ICOS stimulation. BM.564.B6 mice exhibited hallmarks of epitope spreading, including splenic $CD45.1^{+}$ GC B cells (Fig. 4P), altered ANA staining patterns, and WT-derived IgG2c autoreactivity (Fig. 4Q), all of which were diminished in BM.564.ICOS and BM.564.OTII mice. Together, these results suggest that a WT follicular T cell repertoire, but not an OTII-restricted repertoire is sufficient to rescue spontaneous autoreactive GC formation and epitope spreading, suggesting that follicular T cell TCR specificity determines ability to break B cell tolerance.

To distinguish the provision of follicular from GC-extrinsic T cell help, we next used 564Igi;$SAP^{-/-}$ mice, which are still capable of forming GC-independent ASCs (Fig. 1). To establish mice with a TCR-restricted follicular T cell repertoire but still capable of providing GC-extrinsic T cell help, we generated mixed bone marrow chimeras in which irradiated $SAP^{-/-}$;CD45.1 mice were reconstituted with 564Igi;$SAP^{-/-}$ bone marrow and B6;CD45.1

(BM.564-S AP.B6), *SAP*$^{-/-}$;CD45.1 (BM.564-SAP.SAP), or OTII;CD45.1 (BM.564-SAP.OTII) bone marrow (fig. S6A). These chimeras largely phenocopied our observations in ICOS-deficient chimeras, including losses of follicular T cells, activated CD4s, EFO CD4 T cells, and GC B cells that were rescued by a WT, but not restricted OTII, follicular T cell repertoire (fig. S6, B to L). Despite decreases in EFO CD4 T cell numbers and expression of PD1 (fig. S6, I and J), BM.564-S AP.SAP and BM.564-SAP.OTII mice had normal levels of ASCs, CD45.1 enrichment in ASCs, and ASC proliferation (fig. S6, L to N), suggesting that although SAP might be necessary for EFO T cell activation, it is not necessary for ASC generation. BM.564-S AP.SAP and BM.564-SAP. OTII mice also did not have altered ICOSL levels (fig. S6O), indicating that the ICOSL up-regulation observed in BM.564.ICOS mice (Fig. 4O) was specifically due to loss of ICOS signaling rather than general loss of T cell help. Our observations in SAP-deficient chimeras confirm that loss of autoreactive GCs is TCR dependent while also uncovering the presence of a TCR-And ICOS-dependent but SAP- and GC-independent source of ASCs.

T_{FH} and T_{FR} cells from autoreactive GCs recognize autoantigens

After our observations of both follicular TCR dependence of spontaneous autoreactive GC formation and enrichment for a subset of expanded follicular T cell antigen specificities in autoimmune GCs, we next sought to determine the antigen specificity of these TCRs. We hypothesized that TCRs in autoimmune-specific predicted specificity groups bind to autoantigens, facilitating their ability to break B cell tolerance. From our scTCR-seq data, we identified seven orphan TCRs, which we named TCR-A through TCR-G (Fig. 5, A to C), that represent a range of follicular T cell subsets, including both T_{FH} and T_{FR} cells, and predicted specificity groups, clone sizes, and membership to either immunized or autoimmune bone marrow chimeras or both (Fig. 5C). To study these TCRs in vitro, we cloned their full-length TCRαβ sequences and retrovirally expressed each TCR in a TCRα^{-}β^{-} hybridoma with a Nur77–green fluorescent protein (GFP) reporter. TCR-E experienced the greatest Nur77 activation by 564Igi spleen lysates (Fig. 5B and fig. S7A), suggesting that it may be autoreactive.

In parallel, we tested orphan TCR autoreactivity using the peptide major histocompatibility complex (MHC)–TCR chimeric receptor (MCR) coculture system (53). In this system, cognate antigen recognition leads to TCR-specific nuclear factor of activated T cells (NFAT) activation in MCR reporter cells (Fig. 5D) expressing a mouse I-A^{b} MHC class II extracellular domain covalently linked to candidate peptides. Other current methods to identify CD4 T cell cognate peptides are constrained by the relatively lower binding affinity of CD4 TCRs, the variability of peptide binding to MHC class II, and the inability to match randomly mutated artificial peptides to natural peptides and have therefore not succeeded at identifying CD4 autoantigens (54). We used MCR to overcome these challenges using autoimmune bone marrow chimera spleens and kidneys as sources of cDNA to generate a transcriptome-wide library of natural autoantigen peptides (Fig. 5E). We cloned this cDNA-derived peptide (CDP) autoantigen library into the MCR retroviral backbone and transduced NFAT reporter cells to make a murine autoantigen MCR reporter library (MCR-Lib). Coculture of MCR-Lib with each orphan TCR resulted in the greatest MCR activation by TCR-A, TCR-C, TCR-E, and TCR-G (Fig. 5F and fig. S7B), suggesting that these

TCRs may be more autoreactive. Notably, among the seven orphan TCRs identified from scTCR-seq, these were the four TCRs that were more prevalent in the autoimmune follicular T cell repertoire (Fig. 5A). TCR-A and TCR-E were most prevalent in T_{FR} cells, whereas TCR-C and TCR-G were found in T_{FH} clusters (Fig. 5A), suggesting that both T_{FH} and T_{FR} cells may be autoreactive.

To test the reactivity of orphan TCRs, we cocultured MCR-Lib with TCR-A, TCR-B, and TCR-E, and responding MCR reporter cells were enriched through iterative flow sorting (fig. S7C). After six rounds of coculture and sorting, over 50% of MCR reporter cells responded to TCR-A and TCR-E (fig. S7D), whereas TCR-B did not lead to enrichment. Next-generation sequencing identified peptides that were significantly enriched in response to TCR-A or TCR-E coculture relative to the initial MCR-L ib (fig. S7, E and F), suggesting that TCR-A and TCR-E, but not TCR-B, can recognize mouse CDPs. Comparison of peptides enriched after coculture with TCR-A versus TCR-E identified multiple peptides specifically enriched in response to the individual TCRs (fig. S7E), suggesting that TCR-A and TCR-E might recognize distinct antigens and are cross-reactive. Motif analysis of NetMHCIIpan-predicted core binding sequences of MCR-enriched peptides revealed TCR-specific motifs (fig. S7G), likely reflecting nonoverlapping specificity of TCR-A and TCR E. Once we determined that TCR-E is likely autoreactive, we used AlphaFold2 multimer prediction of protein folding to confirm positioning of the TCR-E CDR3αβ sequence in the TCR paratope (fig. S7H).

These results demonstrate not only the ability of our MCR library to detect TCR-specific cross-reactivity from a CDP library of the entire transcriptome but also that disease-specific TCRs may be identified from repertoire-w ide scTCR-seq data using a combination of in silico antigen specificity prediction and in vitro screening for peptide MHC recognition. These findings indicate that TFR cells from autoreactive GCs can both recognize CDPs and are cross-reactive.

A single TFR clone is sufficient to initiate autoreactive GCs

Given the follicular TCR dependence of spontaneous autoreactive GCs and expansion of autoreactive TFR clones in autoimmune chimeras, we next asked whether a singular TCR would be sufficient to initiate autoreactive GCs. To establish mice with a follicular T cell repertoire restricted to our candidate TCRs, we generated retrogenic mice (55) in which full-length TCRαβ sequences identified from scTCR-seq were cloned into a retroviral vector and transduced into *RAG*$^{-/-}$ hematopoietic stem cells (HSCs). Irradiated *Icos*$^{-/-}$;CD45.1 mice were then reconstituted with 564Igi;*Icos*$^{-/-}$ bone marrow mixed with *Icos*$^{-/-}$;CD45.1 bone marrow and either B6 bone marrow or retrogenic HSCs expressing candidate TCRs (Fig. 6A). For these analyses, we chose to test the two most frequent TCRs identified by scTCR-seq (TCR-A and TCR-B) and TCR-E, the most frequent clone identified in both immunized and autoimmune chimeras (Fig. 5A). In this model, autoimmune bone marrow chimeras with retrogenic HSCs (BM.564.TCR-A, BM.564.TCR-B, and BM.564. TCR-E) have follicular T cells with a repertoire restricted to the indicated TCR.

Twelve weeks after reconstitution, we confirmed that ICOS deficiency abrogated follicular T cells and T_{FH} proliferation, which was rescued by inclusion of either a WT follicular T cell

repertoire or a TCR-A– or TCR-E–restricted repertoire, but to a lesser degree with a TCR-B–restricted repertoire (Fig. 6,B and C). Although candidate TCRs restored follicular T cell frequency, they further increased the T_{FH}-to-T_{FR} ratio observed in BM.564.ICOS mice (Fig. 6D), suggesting that TCR specificity can influence T_{FH} and T_{FR} development. We confirmed that the entire T_{FH} compartment was derived from transduced retrogenic cells, whereas CD45.1 cells were still capable of reconstituting the CD4 compartment (fig. S8, A and B). TCR-A–, TCR-B–, or TCR-E–restricted follicular T cell repertoires also rescued T_{reg} frequencies (fig. S8C), suggesting that ICOS-mediated control of the homeostatic T_{reg} pool is TCR dependent. TCR-A rescued the ICOS-dependent increase in naïve CD4 T cells and decrease in EFO CD4 T cells and partially rescued the ICOS-dependent decrease in EFO CD4 T cell expression of CD44 and PD1 (fig. S8, D to I), suggesting that autoreactive follicular T cells can facilitate CD4 T cell activation and EFO T cell responses. These findings indicate that a single autoreactive TCR can not only reconstitute the follicular T cell compartment but also rescue ICOS-dependent changes to CD4 T cell phenotypes in B cell–driven autoimmune disease.

We next asked whether an autoreactive TCR–restricted follicular T cell repertoire was sufficient to rescue spontaneous autoimmune GC formation. BM.564.TCR-A and BM.564.TCR-E mice formed spontaneous GCs, class-switched IgG1 B cells, and ASCs (Fig. 6, E and F), suggesting that a single autoreactive clone is sufficient to initiate autoreactive GCs. BM.564.TCR-A mice had greater GC formation and class switching than BM.564.TCR-B mice (Fig. 6, E and F), suggesting that follicular TCR autoreactivity dictates the extent of spontaneous GC formation. TCR-A–and TCR-E–restricted follicular T cells also rescued $IgD^{-}CD138^{-}GL7^{-}CD38^{+}$ B cell frequency (Fig. 6, G and H), a GC-extrinsic population of B cells that includes both memory B cells and ABCs. As with GC B cells, TCR-B was less capable of rescuing IgD^{-} B cell frequency than autoreactive TCRs (Fig. 6, G and H), suggesting that TCR specificity can shape GC-extrinsic responses as well. Fc receptor-like protein 5 (Fcrl5) and CD23 can distinguish memory B cell populations with distinct spatial localization and recall capacity (56, 57). TCR-A– and TCR-E–restricted follicular T cells not only rescued $Fcrl5^{+}$ memory B cell frequency but also increased $Fcrl5^{+}$ memory B cell frequency beyond what was observed in autoimmune chimeras with a WT follicular T cell repertoire (Fig. 6H), likely reflecting increased GC output driven by an autoreactive TCR. In contrast, decreased ABC frequency was not rescued by TCR-A– or TCR-E–restricted follicular T cells (Fig. 6H), possibly representing decreased EFO CD4 T cell help in the presence of a restricted autoreactive follicular T cell repertoire.

To ask whether a restricted autoreactive follicular T cell repertoire can promote WT B cell entry into spontaneous autoreactive GCs, we identified WT B cells with the congenic marker CD45.1, which is absent from initiating autoreactive 564Igi $CD45.2^{+}$ B cells. TCR-A and TCR-E, but not TCR-B, increased CD45.1 enrichment in the GC B cell but not ASC population (Fig. 6, I and J), indicating that autoreactive follicular T cells are sufficient to promote epitope spreading as measured by WT B cell entry into autoreactive GCs. Notably, although total ASC formation is ICOS and follicular TCR dependent (Fig. 6, F and H), these results suggest that WT B cell entry to the ASC compartment is not. BM.564.TCR-A and BM.564. TCR-E mice also rescued $CD45.1^{+}$ B cell expression of CD21/35, Ki67, CD11c, and CD86, even increasing CD21/35 and CD11c expression beyond what was observed with

a WT repertoire (Fig. 6K). TCR-A and TCR-E but not TCR-B restored splenic CD45.1$^+$ GC B cells and T_{FH} presence within the GC (Fig. 6L). These B cell phenotypic changes suggest that an autoreactive TCR can not only rescue ICOS-dependent loss of B cell activation in autoimmune chimeras but can also drive B cell phenotypes in distinct TCR-specific patterns. We hypothesized that these alterations in B cell phenotype result in downstream changes in ASC and memory B cell phenotypes. TCR-A and TCR-E, but not TCR-B, rescued Ki67 expression in CD45.1$^+$ ASCs (Fig. 6M), although all TCRs were capable of rescuing Fcrl5 expression in CD45.1$^+$IgD$^-$ memory B cells to an even greater extent than with a WT repertoire (Fig. 6N), reflecting autoreactive TCR–specific abilities to not only shape B cell activation but also shape GC output. Together, these results suggest that even a single autoreactive TCR–restricted follicular T cell repertoire can initiate autoreactive GCs, promote memory B cell and ASC formation, and facilitate entry of WT B cells into autoreactive GCs.

Although TCR-A and TCR-E clones were both predominantly found in the TFR cluster by scRNA-seq, they occupied opposite regions of the TFR cluster in transcriptional space (Fig. 5A). We therefore asked whether transcriptional differences, in addition to differences in TCR specificities, might account for the functional differences observed between TCR-A and TCR-E in vivo. Analysis of our scRNA-seq dataset revealed that TCR-A and TCR-E cells were transcriptionally distinct, with increased expression of *Rln3*, *Ms4a4b*, *S100a4*, and *Klf2* in TCR-A and *Hif1a*, *Tpi1*, *Aldoa*, and *Pdcd1* in TCR-E (Fig. 6O). Gene set enrichment analysis of these differentially expressed genes revealed that TCR-A was associated with lymphocyte migration and memory, whereas TCR-E was associated with increase metabolic flux (fig. S8, J to L). Signaling pathway impact analysis (58) reaffirmed these findings, identifying mammalian target of rapamycin (mTOR) signaling as a perturbed pathway in TCR-E (fig. S8L). Intra-TCR differential expression analysis revealed that TCR-E clones from autoimmune chimeras expressed elevated *Cmss1*, *Nav2*, and *Cd72*, whereas TCR-E clones from immunized chimeras expressed elevated *Krt17* (fig. S8, M and N), suggesting that an identical TFR clone can adopt different phenotypes in different immune contexts. These results indicate that although both TCR-A and TCR-E are autoreactive and sufficient to promote autoreactive GCs, they adopt both functional and transcriptional differences in vivo that are context dependent.

TCR diversity and specificity shape epitope spreading

After observing TCR-A– and TCR-E–mediated rescue of spontaneous autoreactive GC formation (Fig. 6L and fig. S8O), we next asked what effect they might have on the autoantibody pool produced in autoimmune chimeras. We hypothesized that an autoreactive TCR–restricted follicular T cell repertoire would facilitate autoantibody epitope spreading but only to a narrow set of autoantigens dictated by the TCR. TCR-A and TCR-E partially rescued ANA reactivity in autoimmune chimeras (Fig. 6P and fig. S8P). Sera from BM.564.B6, BM.564.TCR-A, and BM.564.TCR-E mice exhibited altered ANA staining patterns (Fig. 6P) from the initial 564Igi reactivity (Fig. 1H), indicative of epitope spreading. Interrogation of autoantibody source using WT-specific IgG2c revealed increased ANA reactivity by TCR-A and TCR-E compared with BM.564.ICOS chimeras (Fig. 6P), confirming that the source of autoantibody is not the original 564Igi clone.

Pathogenic autoantibody production was assessed by histologic examination of kidneys from autoimmune chimeras. TCR-A and TCR-E not only rescued but also increased functional autoantibody production resulting in pronounced glomerular IgG and IgG2c deposition (Fig. 6Q and fig. S8Q). Glomerular deposition of autoantibody is usually only appreciable in aged 564Igi mice (45, 46), suggesting that a follicular T cell repertoire restricted to an autoreactive TCR can accelerate pathogenic autoantibody production. These results suggest that TCR autoreactivity is necessary and sufficient for epitope spreading.

To determine the antigen specificity and therefore the breadth of epitope spreading, we tested sera from autoimmune chimeras for the ability to bind to a set of 33 autoantigens using a custom microbead array (Fig. 7A). Principal components analysis of serum autoreactivity separated 564Igi sera from BM.564.B6 sera, whereas sera from retrogenic autoimmune chimeras clustered together with some separation from both 564Igi and BM.564.B6 sera (Fig. 7B), suggesting that TCR specificity can shape the pool of autoantibodies produced. Hierarchical clustering also separated 564Igi sera from BM.564.B6 sera based on autoreactivities and antibody isotype subclass patterns (fig. S9A), confirming broadening of autoantibody specificities in our model. Differential serum autoreactivity analysis of IgG binding revealed the emergence of autoreactivity to a distinct set of autoantigens depending on the follicular T cell repertoire (Fig. 7C). A WT follicular T cell repertoire resulted in the greatest number of reactivities, including reactivity against two tRNA synthetases (Jo1 and EJ) and the systemic sclerosis autoantigen Scl-70 (Fig. 7C). This autoreactivity represents epitope spreading, because it differs from the autoreactivity of 564Igi sera, which is largely toward Ro60/SSA (fig. S9B). In contrast, sera from BM.564.TCR-A, BM.564.TCR-B, and BM.564.TCR-E mice bound to a smaller set of autoantigens (Fig. 7C). When this autoreactivity was compared with autoreactivity in the presence of a WT follicular T cell repertoire, only TCR-A and TCR-E resulted in enrichment and in both cases for only a single autoantigen (fig. S9B). Each TCR also resulted in a unique pattern of epitope spreading. For example, TCR-A sera displayed IgG2c reactivity against Scl-70, thyroglobulin (TG), and Jo1, whereas TCR-B sera lacked IgG2c reactivity to these autoantigens, and TCR-E sera had IgG2c reactivity against only Scl-7 0 and Jo1 (Fig. 7D). Therefore, a diverse follicular TCR repertoire is capable of driving epitope spreading toward a broad set of autoantigens, whereas a restricted autoreactive TCR repertoire can narrow epitope spreading toward a smaller but distinct pool of autoantigens.

DISCUSSION

We have shown that autoreactive follicular T cells are necessary and sufficient to facilitate loss of B cell tolerance and epitope spreading. Even in established chronic autoimmune GCs, continual T cell help was necessary for GC maintenance. Repertoire-w ide analyses revealed that despite expansion of follicular T cells with shared specificities in immunized and autoimmune GCs, we could identify autoimmune-specific TCRs that recognize autoantigens. A follicular T cell repertoire restricted to a single autoreactive TCR was sufficient to rescue spontaneous autoimmune GC formation in ICOS-deficient chimeras, demonstrating the importance of TCR specificity in loss of B cell tolerance. Our findings illustrate the importance of follicular T cell specificity, demonstrating that cognate antigen

identity can influence breadth and direction of epitope spreading, providing a mechanistic link between T cell help and clonal evolution of autoreactive GCs.

Our observation of shared specificities in immunized and autoimmune GCs is consistent with prior reports of T_{FH} and T_{FR} repertoire expansion after immunization with foreign antigens (37, 59, 60). This bystander activation might provide increased coverage for foreign antigen specificity at the expense of potential cross-reactivity with self (61–63). Recent identification in mice and humans of autoreactive conventional $CD4^+$ T cells that escape central tolerance and resemble T_{FH} cells (64) suggests that auto-reactivity might be an evolutionarily adaptive feature of the follicular T cell repertoire. We observed the presence of an autoreactive follicular T cell clone in the repertoire of control immunized mice, suggesting that mechanisms exist to maintain peripheral tolerance of this potentially autoreactive follicular T cell repertoire. Mounting experimental and teleological reasoning suggests that a naïve low-affinity autoreactive B cell pool might also be crucial for functional humoral immunity (6, 65–69). We hypothesize that just as an autoreactive follicular T cell may overcome B cell clonal anergy selective pressures to break B cell tolerance, autoreactive B cells can present autoantigen to cross-reactive follicular T cells to overcome T cell ignorance and break T cell tolerance.

Although B cell maturation, somatic hypermutation, and memory B cell formation occur in the GC, loss of B cell tolerance also occurs at sites other than the GC, such as EFO foci and the marginal zone (70). ASC persistence despite GC deficiency in SAP-deficient mice suggests the existence of a GC extrinsic but ICOS-dependent source of ASC in autoantibody disease. This is consistent with previous reports of ICOS-dependent EFO T cell help in MRL(lpr) mice (71). Given the ability of SAP-deficient T cells to be primed by DCs toward T_{FH} commitment but not form stable T-B conjugates (41–43), we hypothesize that stable T-B interactions and T_{FH} recruitment to the GC might be less necessary for autoreactive ASC development than ICOS-dependent T_{FH} differentiation and development. Although GC, ASC, and memory B cell loss in ICOS-deficient mice was rescued by inclusion of an autoreactive follicular T cell repertoire, only the GC pool had TCR-dependent decreases in WT B cell entry. Neither ICOS nor SAP deficiency altered WT B cell frequency in the ASC pool. Furthermore, an autoreactive TCR could not rescue ICOS-dependent loss of ABCs but increased $Fcrl5^+$ memory B cell frequency. Therefore, we hypothesize that a restricted autoreactive follicular T cell repertoire drives naïve B cell entry into autoreactive GCs, accelerating loss of tolerance, epitope spreading, and memory B cell formation, at the expense of GC-extrinsic pathways of B cell activation. In contrast, WT B cells might use the ABC compartment or marginal zone to bypass GC entry to develop into autoreactive ASCs in the setting of limiting TCR-dependent T cell help, although this process is less efficient than loss of tolerance and epitope spreading in the GC, given the decrease in total ASCs and ABCs.

We show that autoreactive 564Igi B cells are sufficient to break tolerance, but it is possible that other autoreactive B cell receptors (BCRs) with varying avidities and specificities might be either more or less capable of activating autoreactive follicular T cells (72–74). ICOS-, SAP-, and Bcl6-deficient models of loss of T cell help also led to both T_{FH} and T_{FR} deficiency, obscuring the role that each population might individually play in loss

of B cell tolerance. Similarly, retrogenic chimeras necessarily had clonal T_{FH} and T_{FR} repertoires that shared TCR specificity, something we and others rarely observed in a complete follicular T cell repertoire (37, 38), making it difficult for us to distinguish the relative importance of T_{FH} versus T_{FR} specificity in loss of tolerance. Recent studies using inducible and selective T_{FH} or T_{FR} deletion have suggested that T_{FR} rather than T_{FH} cells are responsible for maintaining B cell tolerance (75, 76). Our use of a restricted follicular T cell repertoire also does not replicate the polyclonal bystander T_{FH} and T_{FR} expansion we and others have observed (37, 50), the physiologic relevance of which still remains unclear. When screening for TCR specificity, we limited our pool to autoantigens, although our candidate TCRs might also bind foreign antigens, potentially with greater avidity (63, 77–79). Whether the candidate autoantigens identified by MCR screening can be recognized by these TCRs with high affinity or can induce autoimmune responses in vivo, for example, through immunization, remains to be established. Future experiments will attempt to answer these questions and replicate our findings in other models of B cell autoimmunity.

We conclude that an autoreactive TCR, but not a model TCR, is necessary and sufficient to break B cell tolerance. Implication of follicular T cell specificity in clonal evolution of autoreactive GCs highlights the possibility of using TCR specificity to direct epitope spreading, potentially therapeutically away from self with engineered T cells (80–82). These findings might also extend to other forms of GC dysfunction and loss of B cell tolerance and epitope spreading, such as generation of Epstein-B arr virus and central nervous system cross-reactive TCRs and antibodies in multiple sclerosis (83–86), beneficial B to T_{FH} to CD8 cell cross-talk in cancer or chronic lymphocytic choriomeningitis virus infection (87–89), and autoantibody generation in severe COVID-1 9, multisystem inflammatory syndrome in children, and long COVID (90–96).

MATERIALS AND METHODS

Study design

This study aimed to determine how TCR specificity influences autoreactive GC formation and autoantibody development. We generated genetic mouse models of follicular T cell deficiency and B cell–driven autoimmunity to test the necessity of T cell help for loss of B cell tolerance. We also used retrogenic chimeras to test individual TCRs, cell-based reporters to determine TCR specificity, intravital multiphoton microscopy to visualize follicular T cells in vivo, and scRNA-seq and scTCR-seq analyses to characterize follicular T cell repertoires. Both male and female mice were used for all experiments, and mice were gender and age matched within experiments. For chimera generation, mice were randomly assigned to experimental groups. Experimental and control mice were cohoused whenever appropriate. No statistical methods were used to predetermine sample size. All image quantification was performed in a blind fashion.

Study approval

All animal experiments were conducted in accordance with the guidelines of the Laboratory Animal Center of National Institutes of Health (NIH). The Institutional Animal Care and Use Committee of Harvard Medical School approved all animal protocols (IS111).

Mice

C57BL/6J (B6; #000664), B6.SJL-Ptprc^{a}Pepc^{b}/BoyJ (CD45.1; #002014), B6.129P2-Icos^{tm1Mak}/J (*Icos*$^{-/-}$; #004859), B6.129S6-Sh2d1a^{tm1Pls}/J (*SAP*$^{-/-}$; #025754), B6(129X1)-Tg(Cd4-cre/ERT2)11Gnri/J (*Cd4*^{CreERT2}; #022356), B6.129S(FVB)-Bcl6tm1.1Dent/J (*Bcl6*$^{fl/fl}$; #023727), B6.129P2-Gt(ROSA)26Sortm1(CAG-Brainbow2.1)Cle/J (*R26con/con*; #017492), and B6.129S7-Rag1^{tm1Mom}/J (*RAG*$^{-/-}$; #002216) mice were obtained from the Jackson Laboratories. The 564Igi mice on a C57BL/6 background (46) were provided by T. Imanishi-K ari (Tufts University), and OTII transgenic mice (97) were provided by G. Victora (Rockefeller University) and were maintained in house. All mice were bred and maintained in the Association for Assessment and Accreditation of Laboratory Animal Care–accredited facility at Harvard Medical School at ambient temperature and humidity. Mice were specific pathogen–free and maintained under a 12-hour light/dark cycle with standard chow diet.

Genotyping

564Igi mice were genotyped using digital droplet polymerase chain reaction (PCR). Tail DNA was isolated and digested with Alu I [New England Biolabs (NEB)]. Droplets were prepared from a mix of tail DNA, heavy- or light-chain primers (data file S2) (50), and EvaGreen Supermix (Bio-Rad) using a QX200 Droplet Generator (Bio-R ad). PCR was performed using a C1000 Touch Thermal Cycler (Bio-R ad), and droplets were read on a QX200 Droplet Reader (Bio-R ad). 564Igi heavy- and light-chain copy number was quantified by comparing with amplification of reference mRPP30 using QuantaSoft (Bio-Rad). FACStyping of OTII, CD45.1 mice, and bone marrow chimeras was performed by bleeding mice retroorbitally using heparinized capillary tubes and collecting into 30 μl of acid-citrate-dextrose solution (Sigma-Aldrich). Stabilized blood was underlayered with 1 ml of lymphocyte separation medium (Corning) and centrifuged at 400*g* for 30 min at room temperature. The mononuclear cell layer was aspirated and processed for flow cytometry as described below using anti-CD45.1 and anti-CD45.2 to detect congenic markers or anti-TCR Vα2 to detect OTII T cells. All other genotyping was performed according to the Jackson Laboratory protocols.

Mouse treatments

To generate primary GCs against foreign antigens, mice were immunized either intraperitoneally with 100 μg of NP-OVA (Biosearch) in 50 μl of Hanks' balanced salt solution (HBSS) precipitated in 50 μl of Imject Alum (Thermo Fisher Scientific) or subcutaneously with 25 μg of NP-OVA in 15 μl of HBSS precipitated in 15 μl of Imject Alum per footbed. For immunization of nonautoimmune bone marrow chimeras, primary immunizations were performed 6 weeks after irradiation to allow for hematopoietic reconstitution. To generate secondary responses, nonautoimmune bone marrow chimeras received an intraperitoneal booster immunization of 100 μg of NP-OVA in 100 μl of HBSS 4 weeks after primary immunization. Alternatively, mice were immunized intraperitoneally with 10^{9} sheep red blood cells in 100 μl of HBSS. To induce Cre-mediated recombination, mice were injected intraperitoneally with tamoxifen (50 mg/g; Sigma-Aldrich) in 100 μl of sunflower seed oil (Spectrum Chemical) every 2 days for five total doses. Blood

was collected via cardiac puncture and kept at room temperature for 30 min to promote coagulation and then centrifuged at 1000*g* for 10 min to isolate serum, which was stored at −80°C.

TCR cloning

Retroviral expression plasmids pMSCV–IRES–GFP II (pMIG; #52107) and TCR OTII-2A.pMIG II (pMIG-OTII; #52112) were gifts from D. Vignali (Addgene), and pMSCV-I RES-Ametrine (pMIA) was a gift from J. Moon (Massachusetts General Hospital). Full-length TCRα and TCRβ sequences were identified from scTCR-seq data using Cell Ranger (10X Genomics). Vα sequences with the following Gibson overhangs 5′-CGCCGGAATTCAGATCTACC-3′ and 5′-ATCCAGAACCCAGAACCTGCTG-3′ and Vβ sequences with the following Gibson overhangs 5′-GGAAGAAAACCCCGGTCCCATG-3′ and 5’-GATCTGAGAAATGTGACTCCACCCAAG-3′ (data file S3) were ordered as gene blocks (IDT). T cell receptor alpha constant gene fused to 2A peptide sequence (TRAC-2A) was PCR-amplified from pMIG-OTII using TRAC_F 5′-ATCCAGAACCCAGAACCTGCTG-3′ and 2A_R 5′-CATGGGACCGGGGTT-TTCTTCC-3′. T cell receptor beta constant gene (TRBC) was PCR-amplified from pMIG-OTII using TRBC_F 5′-GATCTGAGAAATGTGACTCCACCCAAG-3′ and TRBC_R 5′-GCGGAATTGATCCCGCTCGAG-3′. Backbone pMIG or pMIA was linearized with Eco RI (NEB) and Xho I (NEB) and combined with the above gel purified inserts into a five-part isothermal assembly using NEBuilder HiFi DNA Assembly Master Mix (NEB) at equimolar ratios. Minipreps were screened by Sanger sequencing, and endotoxin-free Midipreps (Zymo) were inoculated and purified from sequence-verified minipreps.

Cell culture

Human embryonic kidney cells (HEK-2 93T) and mouse embryonic fibroblasts (3T3, NIH) were cultured in Dulbecco’s modified Eagle’s medium (Corning) supplemented with 2 mM l-glutamine, penicillin (100 U/ml), streptomycin (100 μg/ml), and 10% heat-inactivated fetal bovine serum (FBS; Gibco). The $58^{-/-}$ TCR-negative hybridoma cells (98) were a gift from M. Birnbaum (MIT), and A2 TCR-negative hybridoma cells and 16.2C11 reporter cells were gifts from M. Kopf (ETH-Zürich) and described previously (53). The $58^{-/-}$, A2, and 16.2C11 cells were cultured in suspension in RPMI (Corning) supplemented with 2 mM l-glutamine, penicillin (100 U/ml), streptomycin (100 μg/ml), and 10% heat-inactivated FBS. All cells were cultured at 37°C in a 5% CO_2-humidified atmosphere.

Retroviral production and transduction

Retrovirus was produced by transfection of 15×10^6 HEK-293T cells with 20 μg of retroviral plasmid and 20 μg of pCL/Eco (Addgene, #12371) using calcium phosphate (99). After 3 days, supernatant was harvested by centrifugation, titered using 3T3 cells as previously described (100), and stored at −80°C. Nonadherent cells were transduced by resuspending cells in retroviral supernatant at a multiplicity of infection of 0.5 to 2 in non-tissue culture–treated cell culture plates coated with RetroNectin (10 μg/cm^2; Takara) and centrifugation at 800*g* for 2 hours at 30°C. After spinfection, cells were incubated at 32°C for 5 hours, followed by an optional second spinfection. Cells were washed and

replaced with fresh medium after spinfection, and transduction efficiency was assessed 3 days later by flow cytometry.

Bone marrow chimeras

Epitope spreading was induced in an autoreactive B cell–driven model of autoimmunity using mixed 564Igi chimeras as previously described (45). Recipient mice between 8 and 10 weeks old were irradiated with 11 Gy and fed water with sulfamethoxazole/trimethoprim for 10 days to prevent opportunistic infections. Femurs and tibia were dissected from 6- to 8-w eek-old congenic donor mice and rinsed through three rounds of HBSS supplemented with 10 mM Hepes, 1 mM EDTA, and 2% heat-inactivated FBS. Bones were crushed in a mortar and passed through a 70-μm cell strainer (Corning). Bone marrow cells were mixed at indicated ratios, and a total of 15×10^6 cells in 100 μl were injected intravenously into each irradiated recipient 8 to 10 hours after irradiation. Six weeks after reconstitution, chimerism was verified by FACStyping as described above.

Retrogenic chimeras

Retrogenic chimeras were used to create restricted T cell repertoires using candidate TCRs (55). Bone marrow cells were isolated from *RAG*$^{-/-}$ mice as described above. HSCs were purified using the MojoSort Mouse CD117 Selection Kit (BioLegend) following the manufacturer's protocol. Postsort purity was verified by flow cytometry, and HSCs were resuspended at 1×10^6 cells/ml in RPMI supplemented with 2 mM l-glutamine, penicillin (100 U/ml), streptomycin (100 μg/ml), 10% heat-inactivated FBS, 20 mM Hepes, 50 μM β-mercaptoethanol, 1 mM sodium pyruvate, 100 μM nonessential amino acids (complete RPMI), interleukin-3 (IL-3; 20 ng/ml; PeproTech), IL-6 (50 ng/ml; PeproTech), and stem cell factor (SCF) (50 ng/ml; PeproTech). HSCs were cultured at 37°C in a 5% CO_2-humidified atmosphere for 24 hours, followed by spinfection with TCR-Expressing retrovirus as described above. Transduced *RAG*$^{-/-}$ HSCs were washed, and 1×10^6 cells were included in bone marrow mixes to reconstitute irradiated mice as described above.

Flow cytometry

Spleens and lymph nodes were harvested into ice-cold fluorescence-activated cell sorting (FACS) buffer [phosphate-buffered saline (PBS) with 0.5% heat-inactivated FBS, 1 mM EDTA, and 0.05% sodium azide] and mechanically digested through a 70-μm cell strainer (Corning). Spleens were incubated in red blood cell lysis buffer (155 mM NH_4Cl, 12 mM $NaHCO_3$, and 0.1 mM EDTA) for 3 min at room temperature and washed with FACS buffer. Cells were counted, and 1×10^6 cells per well were added to round-bottom 96-well plates and incubated with 50 μl of staining mix (appropriate antibodies and viability dye in FACS buffer) for 30 min on ice. Antibodies that were used are listed in data file S4. Plates were washed with FACS buffer and, for two-step staining procedures, incubated with 50 μl of secondary staining mix (appropriate streptavidin antibody in FACS buffer) for 15 min on ice. For intracellular staining, cells were fixed with fixation/permeabilization buffer (eBioscience) for 30 min at room temperature, washed with permeabilization buffer (eBioscience), and incubated with 50 μl of intracellular staining mix (appropriate intracellular antibody in permeabilization buffer) for 30 min at room temperature. Cells were washed with a final wash of FACS buffer, resuspended in 150 μl of FACS buffer, and read

using three-to eight-fluorophore flow cytometry on a FACSCanto II (BD Biosciences) with 488-, 405-, and 640-nm lasers using FACSDiva (BD Biosciences). Flow cytometry gating strategies are shown in fig. S10. Two-w ay purity sorts were performed using a FACSAria II (BD Biosciences) with 355-, 405-, 488-, 640-, and 592-nm lasers into complete RPMI. Postsort purity was verified by flow cytometry. Compensation matrices were determined using unstained and single fluorophore–stained controls. Data were analyzed using FlowJo (BD Biosciences).

Intravital multiphoton microscopy

Mice were anesthetized by inhalation of 2% isoflurane in 100% oxygen and maintained with 0.5 to 1% isoflurane monitored by pedal withdrawal reflex and respiratory rate. Mice were restrained on a stage warmer, and a ventral midline incision was made. The lateral skin was separated from the peritoneum by gentle blunt dissection, and the inguinal lymph node was exposed by removal of overlying fat and restrained under a coverslip using vacuum grease (VWR). To label FDCs, mice were injected intravenously with 3 μg of PE anti-C D21/35 (BioLegend, 7E9) 2 days before imaging. All imaging was performed on an upright Olympus FV1200 MPE multiphoton system microscope fitted with a 20× 0.95 numerical aperture plan water-immersion objective, a MaiTai HP DeepSee Ti-Sapphire laser (Spectra-Physics), and four nondescanned detectors (two GaAsP and two regular photomultiplier tubes). Imaging was performed using λ = 920-nm excitation, and emission was collected in three channels, using the following filter sets: a pair of cyan fluorescent protein (CFP) (480/40 nm) and yellow fluorescent protein (YFP) (525/50 nm) filters, separated by a 505-n m dichroic mirror, for CFP/GFP/YFP detection, and a third filter (605/70 nm) for red fluorescent protein detection. Second harmonic generation by collagen was detected in the CFP filter. Movies were acquired as 75-μm Z-stacks with 15-μm Z resolution and 800 × 800 X-Y resolution at ~30 s per frame. Images were analyzed using Fiji (ImageJ).

Immunofluorescence confocal microscopy

Spleens were perfused with PBS, followed by 2% paraformaldehyde (Electron Microscopy Sciences) in PBS. Tissues were fixed in 2% paraformaldehyde for 8 hours at 4°C, cryoprotected with 30% sucrose in PBS overnight at 4°C, perfused with 30% OCT (Tissue-Tek) in PBS, embedded in 100% OCT in Standard Cryomolds (Tissue-Tek) in the vapor phase of liquid nitrogen, and stored at −80°C. Frozen sections were cut on a cryostat at a thickness of 20 μm and allowed to dry for 60 min at room temperature. Sections were fixed with acetone for 5 min at −20°C, then permeabilized, and blocked with 5% normal rat serum (Thermo Fisher Scientific) in immunofluorescence (IF) buffer [PBS with 0.2% bovine serum albumin (BSA) and 0.3% Triton X-100] for 1 hour at room temperature. Slides were stained with primary antibody in IF buffer overnight at 4°C and secondary antibody or streptavidin-c onjugated fluorophore in IF buffer for 4 hours at room temperature where appropriate. Antibodies that were used are listed in data file S4. Slides were stained with 4′,6-diamidino2-phenylindole (DAPI; 2 μg/ml) where indicated and mounted using Fluoro-Gel (Electron Microscopy Sciences). Images were acquired using a FLUOVIEW FV3000 confocal laser scanning microscope (Olympus) with 10× or 30× objectives and analyzed using Fiji (ImageJ).

Antinuclear IF

ANA-H Ep-2 slides (Aesku) were brought to room temperature and incubated with 30 μl of sera diluted 1:20 in PBS for 1 hour at room temperature. Slides were blocked with 0.5% BSA and 0.1% Tween 20 in PBS and stained with secondary antibody for 1 hour at room temperature. The following secondary antibodies and stains were used: Alexa Fluor 488 (AF488) anti-m ouse IgG (SouthernBiotech; 1:400), AF488 anti-mouse IgG2c (SouthernBiotech; 1:400), and AF594 cholera toxin subunit B (Thermo Fisher Scientific). Slides were then stained with DAPI (2 μg/ml) and mounted using Fluoro-Gel (Electron Microscopy Sciences). Images were acquired using a FLUOVIEW FV3000 confocal laser scanning microscope (Olympus) with a 30× objective and analyzed using Fiji (ImageJ).

Nur77 reporter hybridoma

Nr4a1-GFP bacterial artificial chromosome (BAC) (101) (GENSAT1-BX1262, BacPac Genomics) was linearized with PI–Sce I (NEB) and purified by two-dimensional gel electrophoresis. Electroporation was performed by resuspending 1×10^6 $58^{-/-}$ cells in 100 μl of Ingenio Electroporation Solution (Mirus) and subjecting cells to 140 V at 950 μF and infinite resistance in 0.2-cm Gene Pulser cuvettes (Bio-Rad). After 2 weeks, cells were pulsed with Cell Stimulation Cocktail (eBioscience), and GFP-positive cells were flow-sorted as described above. Single-cell clones were selected by limiting dilution and screened individually again. Clone 58.2E7 was selected for high GFP upregulation with low background activation and used as a TCR-negative hybridoma for future experiments.

MCR autoantigen library construction

Total RNA was isolated from the spleen and kidney from autoimmune chimeras using the RNeasy Plus Mini Kit (QIAGEN) following the manufacturer's protocols. RNA was treated with QIAseq FastSelect - rRNA HMR (QIAGEN) to remove ribosomal RNA before double-stranded cDNA (dscDNA) synthesis was performed using the Maxima H Minus Double-S tranded cDNA Synthesis Kit (Thermo Fisher Scientific) following the manufacturer's protocols. A CDP library was generated by randomly fragmenting dscDNA using the DNA Fragmentation Kit (Takara) for 8 min. Vector homologous adaptors were generated by PCR using MHCR2leader 5′-CAAC-CATGGCTCTGCAGA-3′ and 5′linker3′o 5′-GGAACCGCCCTCA-GTCCTTG-3′ or 3′linker5′o 5′-GGAGGATCCGGTGGTAGCGG-3′, and PepSeq1 5′-CCGTTGGTGAAGTAGCACTC-3′ from the MCR backbone plasmid pMY-MCR2-I-A^b (pMY-MCR) (53) and ligated to fragmented dscDNA. Inserts were size-s elected by gel electrophoresis, PCR-amplified using MHCR2leader and PepSeq, and cloned into pMY-MCR linearized with Bmr I (NEB) using NEBuilder HiFi DNA Assembly Master Mix (NEB) at equimolar ratios. DNA assembly products were electroporated into MegaX DH10B T1R Eelctrocomp Cells (Thermo Fisher Scientific) generating over 3×10^7 clones, providing transcriptome-wide coverage of most peptides (53). 16.2C11 reporter cells were transduced with this library as described above, and IA/IE$^+$NFAT-Blue$^-$ cells were sorted by FACS as described above. To eliminate cross-reactive peptides, sorted reporter cells expressing the autoantigen library were cocultured with a 10-fold excess of naïve polyclonal B6 CD4 T cells for 8 hours, and NFAT-Blue$^-$ cells were sorted and expanded for a final complexity of ~1×10^7 (MCR-Lib).

TCR hybridoma generation and coculture

A2 and 58.2E7 cells were transduced by spinfection with retrovirus expressing candidate TCRs as described above. Three days after transduction, TCRβ and ametrine-expressing cells were flow-sorted as described above. To assess TCR binding, 58.2E7 cells were cocultured with anti-CD3 (2 μg/ml) and anti-CD28 (1 μg/ml) or a fivefold excess of antigen-presenting cells (APCs) from indicated tissues for 12 hours, and Nur77-G FP reporter activity was measured by flow cytometry. For autoantigen screening, MCR-L ib cells were cocultured with a fivefold excess orphan TCR-expressing A2 cells in 96-well U-bottom plates at 1×10^5 total cells per well. After 12 hours, ametrine$^-$GFP$^+$NFAT-Blue$^+$ cells were sorted as described above and expanded. After six rounds of iterative coculture and sorting, DNA was isolated from sorted reporter cells, and the peptide sequence of the MCR construct was PCR-amplified using MHCR2leader and PepSeq1. This fragment was cloned into pMY-MCR linearized with Bmr I using NEBuilder HiFi DNA Assembly Master Mix and sequenced by Sanger sequencing using IRES_F 5′-GTGCCAC-GTTGTGAGTTGGATAG-3′. Cognate antigen was identified by comparing sequencing results with the mouse transcriptome using Nucleotide BLAST (NIH; https://blast.ncbi.nlm.nih.gov/).

Next-generation sequencing of MCR peptide library

To determine the entire peptidome of starting and enriched MCR libraries, genomic DNA was isolated from MCR cells using the DNeasy Blood & Tissue Kit (QIAGEN) with ribonuclease A (QIAGEN) before treatment. Next-generation sequencing libraries were prepared by a two-step PCR protocol. First, MCR peptide sequences were PCR-amplified from 5 μg of genomic DNA using PCR1_ MCR_F 5′-TCTTGTGGAAAGGACGAAACACCGGCTGCTGTG GTGGTGCTGATGG-3′ and PCR1_MCR_R 5′-TCTACTATTCTTTCCCCTGCACTGTCCGTTGGTGAAGTAGCACTC-3′ with NEBNext Ultra II Q5 Master Mix (NEB) in a 50-μl reaction for 15 to 35 cycles. Cycle counts necessary to reach but not exceed the linear range were determined by quantitative real-time PCR (qRT-PCR) with SYBR Green Supermix (Bio-Rad). PCR products were pooled when multiple reactions were performed for the same sample, concentrated using DNA Clean & Concentrator (Zymo), and size-s elected by gel electrophoresis and extraction (QIAGEN). Purified products were diluted, and 1 ng of each sample was PCR-amplified using unique barcoded sequencing adapters PCR2_Fx 5′-AATGATACGGCGA CCACCGAGATCTACAC[barcode]ACACTCTTTCCCTACACG ACGCTCTTCCGATCT[stagger]TCTTGTGGAAAGGACGAAA-CACCG-3′ and PCR_Rx 5′-CAAGCAGAAGACGGCATACGAGA T[barcode]GTGACTGGAGTTCAGACGTGTGCTCTTCCGATCT[stagger]TCTACTATTC TTTCCCCTGCACTGT-3′ with Q5 Hot Start High-Fidelity 2X Master Mix (NEB) for 16 cycles. Libraries were purified using AMPure XP Beads (Beckman Coulter), quantified by qRT-PCR using i5_F 5′-AATGATACGGCGACCACCGAG ATCTACAC-3′ and i7_R 5′-CAAGCAGAAGACGGCATACGAGAT-3′, and pooled to equimolar ratios. After TapeStation quality control (Agilent), libraries were sequenced on a NextSeq 500 (Illumina).

MCR peptide analysis

Open reading frames (ORFs) were determined from raw FASTA files using orfipy (version 0.0.4) (102) with a minimum length of 60 nucleotides. MCR peptide sequences were extracted from ORFs as peptide sequences flanked by the amino acid sequences PRTE and SGGS using str_match from tidyverse (version 2.0.0). Peptide enrichment was calculated for each individual peptide in each individual sample based on fold change (*FC*)

$$FC = \frac{n_x^i / n_x^{\text{total}}}{n_{\text{ref}}^i / n_{\text{ref}}^{\text{total}}}$$

where n_x^i and n_{ref}^i represent the number of reads n corresponding to peptide i in sample x or the entire library ref and n_x^{total} and $n_{\text{ref}}^{\text{total}}$ represent the total number of reads corresponding to any peptide in sample x or the entire library ref. Differential analysis was performed on a subset of peptides that each represented at least 0.01% of the test peptide library. Gene identity was mapped to individual peptides using blastp-short from BLAST+ (version 2.12.0) with the RefSeq mouse proteome (https://ftp.ncbi.nlm.nih.gov/refseq/M_musculus/mRNA_Prot), and the highest scoring gene by bitscore was matched with each peptide and annotated using biomaRt (version 3.16). MHC class II–predictive binding scores were calculated using NetMHCIIpan (version 4.1) (103), and an aggregate score was calculated as the sum of eluted ligand (EL) and binding affinity (BA) scores for H2-IAb, H2-IAd, and H2-IEd.

Autoantigen array

Autoantigen arrays were generated, and assays using the arrays were performed as described previously (104). Briefly, 1×10^6 carboxylated magnetic beads per ID (MagPlex-C, Luminex) were distributed into 96-well plates (Greiner BioOne), washed, and resuspended in phosphate buffer (0.1 M NaH_2PO_4; pH 6.2) on a 96-well plate magnet. Bead surface was activated by addition of 100 μl of phosphate buffer containing 0.5 mg of 1-e thyl-3(3-dimethylamino-propyl)carbodiimide (Pierce) and 0.5 mg of *N*-hydroxysuccinimide (Pierce). After 20 min of incubation on a shaker (Grant Bio), beads were washed and resuspended in activation buffer (0.05 M MES; pH 5.0). Eight micrograms of each analyte (data file S5) and control antibody were diluted in PBS, transferred into 96-w ell plates, and then mixed with activated beads for coupling during a 2-h our incubation at room temperature. Beads were washed three times in 100 μl of storage buffer [0.02% Tween 20 in PBS (PBS-T), 0.1% BSA, and 0.05% sodium azide], resuspended in 50 μl of storage buffer, and stored in plates at 4°C overnight. Immobilization of the antigens was confirmed, and the assay conditions were optimized by analysis using commercially available mouse monoclonal antibodies or antibodies specific for 6× histidine epitope tags (ab9108). Prototype human plasma samples were used for validation of bead arrays. Mouse sera were diluted 1:100 in an assay buffer of 0.05% PBS-T supplemented with 3% (w/v) BSA (Sigma-Aldrich) and transferred into a 96-well plate. The bead array was distributed into a 384-w ell plate (Greiner BioOne) by transfer of 5 μl of bead array per well, and then 45 μl of the diluted sera were aliquoted and transferred into the 384-well plate. Samples were incubated for 90 min on a shaker (Grant Bio) at room temperature. Beads were washed three times with 60

μl of PBS-T on a plate washer (EL406, BioTek). Secondary antibodies, including 50 μl of R-phycoerythrin (PE)–conjugated Fcγ fragment–specific goat anti-mouse IgG (115–116-071, the Jackson Laboratories), R-PE–conjugated Fcγ subclass 2a–specific goat anti-mouse IgG (115–005-206, the Jackson Laboratories), and R-P E–conjugated Fcγ subclass 2c–specific goat anti-mouse IgG (115–005-208, the Jackson Laboratories), were diluted 1:500, 1:1000, and 1:1000, respectively, in 3% BSA in 0.05% PBS-T based on optimized assay conditions and transferred to three separate 384-w ell plates. After incubation with the secondary antibody for 45 min, plates were washed three times with 60 μl of PBS-T and resuspended in 50 μl of PBS-T for readout in a FlexMap3D instrument (Luminex Corp). Principal components analysis and clustering were performed on median fluorescence intensity (MFI) values for each antigen using prcomp from stats (version 3.6.2) with scaled variables and visualized using autoplot from ggfortify (version 0.4.14).

Single-cell RNA sequencing

Raw scRNA-seq data were obtained from Gene Expression Omnibus (GEO) (www.ncbi.nlm.nih.gov/geo/query/acc.cgi?acc=GSE157649). The Cell Ranger (10X Genomics, version 7.0.0) multipipeline was used to align 5′ gene expression reads to the GRCm39 reference genome (mm39). Only barcodes with unique molecular identifier counts that passed the threshold for cell detection were included in gene-barcode matrices. Individual sample matrices were loaded in Seurat (version 4.2.0) (105) using the Read10X function and filtered for cells with at least 200 genes detected and genes detected in at least three cells using the CreateSeuratObject function. Individual samples were merged using the merge function, and S and G_2-M cell cycle phase scoring was assigned using CellCycleScoring. To remove batch effects between samples associated with a heat shock gene expression signature, genes annotated with the Gene Ontology biological process (GOBP) term “cellular response to heat” (GO:0034605) were used to assign a heat shock score using AddModuleScore. Cells with less than 800 or greater than 3500 genes detected, less than 2000 reads detected, greater than 7% mitochondrial RNA content, greater than 20% ribosomal RNA content, an S phase score greater than 0.15, or a G_2-M phase score greater than 0.15 were excluded from analysis. BCR and TCR variable and constant genes were excluded from scRNA-seq analysis to prevent clustering based on V(D)J transcripts. Data were normalized and scaled using NormalizeData and ScaleData in Seurat to regress out mitochondrial RNA content, ribosomal RNA content, number of unique molecular identifiers, and heat shock score before correcting for batch effects using Harmony (version 0.1.0) (106). After Harmony integration, clusters were identified using FindClusters to apply shared nearest neighbor–based clustering using the first 20 principal components with k = 30 and resolution = 0.3. The same Harmony embeddings were used to generate Uniform Manifold Approximation and Projection (UMAP) projections. Clusters were annotated on the basis of expression of marker genes, including *Foxp3* (T_{FR}), *Sostdc1* (Sostdc1), *Tcf7* [T_{FH}–T cell factor 1 (Tcf1)], *Tigit* (T_{FH}-exhausted), *S100a6* (T_{FH}-activated), *Sell* [T_{FH}–central memory (CM)], *Gzmk* (T_{FH}-effector), and *Isg15* [T_{FH}–interferon-stimulated gene (ISG)]. Cluster determination was confirmed by identifying differentially expressed marker genes for each cluster using FindAllMarkers with the MAST (107) algorithm and comparing with known cell type–specific marker genes. Cluster names were updated using RenameIdents. Differentially expressed genes between autoimmune or nonautoimmune

chimeras were determined using FindMarkers with the MAST algorithm across all genes. For differential expression analysis within individual clusters or clonotypes, Seurat objects were first subset using the subset function.

Gene set enrichment and pathway analysis

Pathway analysis and gene set enrichment analysis were performed using clusterProfiler (version 4.6.0) (108). Differentially expressed genes were ranked according to $\log_2$ fold change ($\log_2$FC) for enrichment analysis. Ranked gene lists were used to query GOBP (109, 110) and MSigDB (version 2022.1.Mm) (111, 112) signature libraries. Signaling pathway impact analysis (version 2.50.0) (58) was used to identify significantly altered pathways based on topology using differentially expressed genes ($P_{adj} < 0.05$).

Single-cell T cell receptor sequencing

Raw scTCR-seq data were obtained from GEO (www.ncbi.nlm.nih.gov/geo/query/acc.cgi?acc=GSE157649). The Cell Ranger (10X Genomics, version 7.0.0) multipipeline was used to align TCR reads to the GRCm39 reference genome (mm39). Only TCRs with full-length and productive α and β chain sequences were included in analysis. Clonotypes were determined by grouping cell barcodes that shared the same pair of productive CDR3α and CDR3β amino acid sequences, and clone size was calculated by the number of unique cell barcodes belonging to an individual clonotype. Clonality was matched with gene expression analysis in Seurat by adding clonality information to the metadata using AddMetaData based on cell barcodes. Unweighted TCR network analysis between samples and conditions was performed using the qgraph package (version 1.9.2). TRSSs were computed using the Battacharyya coefficient (*BC*) (113):

$$BC_{i,j} = \sum_{k=1}^{C} \sqrt{p_k^i \bullet p_k^j}$$

where p_k^i and p_k^j are the proportions of cells in groups i and j that belong to clonotype k, with a total of C clonotypes.

Grouping of lymphocyte interactions by paratope hotspots

GLIPH2 (114) clusters TCRs on the basis of a global similarity index, determined by CDR3 sequences that differ by up to one amino acid, and a local similarity index, determined by common CDR3 motifs of two to three amino acids. The GLIPH2 mouse CD4 dataset was used for reference. Fisher's exact test was used to assess the statistical significance of a given motif, and specificity groups were filtered for global clusters with Fisher score of <0.05. Specificity group prediction was matched with gene expression analysis based on clonotype sequences.

Geometric Isometry–based TCR Alignment Algorithm

GIANA4 (version 4.1) (115) clusters TCRs with predicted shared antigen specificity in Euclidean space based on BLOSUM62 isometric encoding of CDR3β amino acids. GIANA was performed using GIANA4.1.py with a Smith-Waterman alignment threshold of 10

and an isometric distance cutoff of 10. Principal components analysis and clustering were performed on scaled isometric coordinates using *k*-means from stats (version 3.6.2) with $k = 20$ and visualized using autoplot from ggfortify (version 0.4.14). Specificity group prediction was matched with gene expression analysis based on CDR3β sequences.

TCRdist3

TCRdist3 (version 0.2.2) (116) groups TCRs into predicted antigen–specific metaclonotypes using a distance metric based on TCRβ biochemistry. Murine TRBV sequences were annotated manually to match IMGT allele names (www.imgt.org/vquest/refseqh.html). Intraclone distances were calculated using TCRrep, and interrepertoire distances were calculated using compute_rect_distances. Clustering and metaclonotype annotation were performed on the basis of probability of V(D)Jβ generation using OLGA (117) modeled TCR generation and TCRdist3 radius = 50. Multidimensional scaling was performed on the symmetric intraclone distance matrix using cmdscale from stats (version 3.6.2), and public (in >1 sample) clones were visualized. Specificity group prediction was matched with gene expression analysis based on clonotype sequences.

TCR intrinsic regulatory potential

TiRP scoring uses features of individual TCRs to predict T cell fate (51). mTiRP is the greatest contributor to T_{reg} fate (51) and therefore was used as an estimate for autoreactivity. TiRP scores were computed from scTCR-seq data for each clone using CDR3β sequence and TRBV gene. TiRP scores were matched with gene expression analysis based on clonotype sequences.

DeepTCR2

DeepTCR2 (version 2.1.0) (118) classifies both repertoires and antigen-specificity based on machine learning featurization of TCRαβ sequences using an unsupervised deep neural network. TCR featurization was performed using a variable autoencoder (VAE) with 256 latent dimensions, $k = 5$ for the first convolutional layer of the graph, learned latent dimensionality of 64 for amino acids, learned latent dimensionality of 48 for V(D)J genes, latent alpha of 0.001, and three convolutional layers with 32, 64, and 128 neurons, respectively. The VAE was trained using an Adam Optimizer with learning rate = 0.001 until convergence criteria of >0.01 decrease in determined interval were met. UMAP was calculated using unsupervised sequence featurization, and expanded (>10 cells) clones were visualized. For sample-agnostic clustering, a dendrogram was constructed to compare clonotype distribution in UMAP space and PhenoGraph clustering using Kullback-Leibler divergence. Specificity group prediction was matched with gene expression analysis based on clonotype sequences.

AlphaFold2

AlphaFold (version 2.1.1) (119) multimer was used to predict TCRαβ structures. AlphaFold2 was performed using full-length TCRα and TCRβ sequences identified by the Cell Ranger (10X Genomics, version 7.0.0) multi pipeline and a mouse UniProt database (www.uniprot.org/uniprotkb/?query=*). Top ranked prediction was used for visualization.

Image quantification

Confetti allele clonality was calculated using color dominance as previously described (49). Briefly, color dominance in $Cd4^{CreERT2};R26^{con/con}$ mice was quantified in multiple Z planes. GCs were identified on the basis of CD21/35 staining for FDCs. Cells of each color recombination were counted manually in either the GC or adjacent regions. HEp-2 staining was quantified using CellProfiler (120). Nuclear masks were created using DAPI with IdentifyPrimaryObjects, and cytoplasm masks were created by subtracting DAPI staining from cholera toxin subunit B staining with IdentifySecondaryObjects. IgG or IgG2c MFI was calculated using MeasureObjectIntensity. Glomerular antibody deposition was quantified using Fiji (ImageJ). Glomerular masks were created using CD31 staining, and IgG or IgG2c MFI was measured within each mask using Multi Measure. Follicles were defined using CD169 staining, and an average number of GCs per follicle were calculated for each sample. GC size was calculated using Fiji (ImageJ).

Visualization

Bar graphs were created using ggpubr (version 0.4.0.999) or Prism (GraphPad, version 9.4.1), and scatter plots were created using ggplot2 (version 3.3.6). Gene set enrichment plots were generated using clusterProfiler (version 4.6.0). Heatmaps and hierarchical clustering were performed using pheatmap (version 1.0.12). UMAP plots were generated using Seurat. Peptide motifs were created using ggseqlogo (version 0.1). Protein structures were visualized using ChimeraX (UCSF, version 1.5). Experimental diagrams and schematics were created with BioRender.com.

Statistical analyses

All values are expressed as means ± SD. Measurements were taken from distinct samples. Statistical significance was determined using two-tailed Student's t test for two-w ay comparisons or one-way analysis of variance (ANOVA) for grouped comparisons. Two-sided testing with $\alpha = 0.05$ was used. We corrected for multiple comparisons and report adjusted P values using Bonferroni correction. For pathway analyses, Fisher's exact test was used with Benjamini-Hochberg correction for multiple testing.

Supplementary Material

Refer to Web version on PubMed Central for supplementary material.

Acknowledgments:

We thank H. Leung of the Optical Microscopy Core and J. Moore, V. Haridas, and A. Agarwal of the Flow and Imaging Cytometry Resource at the PCMM for technical assistance. We thank M. Birnbaum, B. Smith, and J. Moon for providing critical reagents. We thank H. Cantor, D. Mathis, and J. Moon for helpful conceptual advice.

Funding:

This study was supported by the NIH (T32GM007753, T32GM144273, T32AI007529, and F30AI160909 to E.H.A.-G.; T32MH019938 to T.R.P.; and R01AR074105, R01AI130307, and R01AR072965 to M.C.C.), the Henry Gustav Floren Family Trust (to P.J.U.) and the Stanford Department of Medicine Team Science Program (to P.J.U.).

Data and materials availability:

All scRNA-seq and scTCR-seq have been deposited in the GEO database and are available under primary accession number GSE157649 (www.ncbi.nlm.nih.gov/geo/query/acc.cgi?acc=GSE157649). Connective tissue disease autoantigen array data have been deposited in the GEO database and are available under primary accession number GSE231808 (www.ncbi.nlm.nih.gov/geo/query/acc.cgi?acc=GSE231808). Relevant code and processed data are available through GitHub (https://github.com/egarren/scTCR). 58.2E7 cells are available upon request. All TCR plasmids described herein have been deposited in Addgene. All transgenic mice used in this study are available through the Jackson Laboratories. Raw data used to generate figures are presented in data file S1.

REFERENCES AND NOTES

1. Mueller DL, Mechanisms maintaining peripheral tolerance. Nat. Immunol. 11, 21–27 (2010). [PubMed: 20016506]
2. Brooks JF, Murphy PR, Barber JEM, Wells JW, Steptoe RJ, Peripheral tolerance checkpoints imposed by ubiquitous antigen expression limit antigen-specific b cell responses under strongly immunogenic conditions. J. Immunol. 205, 1239–1247 (2020). [PubMed: 32709661]
3. Mayer CT, Nieke JP, Gazumyan A, Cipolla M, Wang Q, Oliveira TY, Ramos V, Monette S, Li Q-Z, Gershwin ME, Kashkar H, Nussenzweig MC, An apoptosisdependent checkpoint for autoimmunity in memory B and plasma cells. Proc. Natl. Acad. Sci. 117, 24957–24963 (2020). [PubMed: 32963096]
4. Pike BL, Boyd AW, Nossal GJ, Clonal anergy: The universally anergic B lymphocyte. Proc. Natl. Acad. Sci. U.S.A. 79, 2013–2017 (1982). [PubMed: 6804951]
5. Cornall RJ, Goodnow CC, Cyster JG, The regulation of self-reactive B cells. Curr. Opin. Immunol. 7, 804–811 (1995). [PubMed: 8679124]
6. Burnett DL, Reed JH, Christ D, Goodnow CC, Clonal redemption and clonal anergy as mechanisms to balance B cell tolerance and immunity. Immunol. Rev. 292, 61–75 (2019). [PubMed: 31556969]
7. Reed JH, Jackson J, Christ D, Goodnow CC, Clonal redemption of autoantibodies by somatic hypermutation away from self-reactivity during human immunization. J. Exp. Med. 213, 1255–1265 (2016). [PubMed: 27298445]
8. Vinuesa CG, Cook MC, Angelucci C, Athanasopoulos V, Rui L, Hill KM, Yu D, Domaschenz H, Whittle B, Lambe T, Roberts IS, Copley RR, Bell JI, Cornall RJ, Goodnow CC, A RING-type ubiquitin ligase family member required to repress follicular helper T cells and autoimmunity. Nature 435, 452–458 (2005). [PubMed: 15917799]
9. Mietzner B, Tsuiji M, Scheid J, Velinzon K, Tiller T, Abraham K, Gonzalez JB, Pascual V, Stichweh D, Wardemann H, Nussenzweig MC, Autoreactive IgG memory antibodies in patients with systemic lupus erythematosus arise from nonreactive and polyreactive precursors. Proc. Natl. Acad. Sci. U.S.A. 105, 9727–9732 (2008). [PubMed: 18621685]
10. Sabouri Z, Schofield P, Horikawa K, Spierings E, Kipling D, Randall KL, Langley D, Roome B, Vazquez-Lombardi R, Rouet R, Hermes J, Chan TD, Brink R, Dunn-Walters DK, Christ D, Goodnow CC, Redemption of autoantibodies on anergic B cells by variable-region glycosylation and mutation away from self-reactivity. Proc. Natl. Acad. Sci. U.S.A. 111, E2567–E2575 (2014). [PubMed: 24821781]
11. Allen CDC, Okada T, Cyster JG, Germinal-center organization and cellular dynamics. Immunity 27, 190–202 (2007). [PubMed: 17723214]
12. Crotty S, T follicular helper cell differentiation, function, and roles in disease. Immunity 41, 529–542 (2014). [PubMed: 25367570]
13. Akama-Garren EH, Carroll MC, T cell help in the autoreactive germinal center. Scand. J. Immunol. 95, e13192 (2022). [PubMed: 35587582]

14. Chen P-M, Tsokos GC, The role of CD8+T-cell systemic lupus erythematosus pathogenesis: An update. Curr. Opin. Rheumatol. 33, 586–591 (2021). [PubMed: 34183542]
15. Kim SJ, Lee K, Diamond B, Follicular helper T cells in systemic lupus erythematosus. Front. Immunol. 9, 1793 (2018). [PubMed: 30123218]
16. Simpson N, Gatenby PA, Wilson A, Malik S, Fulcher DA, Tangye SG, Manku H, Vyse TJ, Roncador G, Huttley GA, Goodnow CC, Vinuesa CG, Cook MC, Expansion of circulating T cells resembling follicular helper T cells is a fixed phenotype that identifies a subset of severe systemic lupus erythematosus. Arthritis Rheum. 62, 234–244 (2010). [PubMed: 20039395]
17. Yang J-H, Zhang J, Cai Q, Zhao D-B, Wang J, Guo P-E, Liu L, Han X-H, Shen Q, Expression and function of inducible costimulator on peripheral blood T cells in patients with systemic lupus erythematosus. Rheumatology (Oxford) 44, 1245–1254 (2005). [PubMed: 15987711]
18. Tzartos JS, Craner MJ, Friese MA, Jakobsen KB, Newcombe J, Esiri MM, Fugger L, IL-21 and IL-21 receptor expression in lymphocytes and neurons in multiple sclerosis brain. Am. J. Pathol. 178, 794–802 (2011). [PubMed: 21281812]
19. Saito R, Onodera H, Tago H, Suzuki Y, Shimizu M, Matsumura Y, Kondo T, Itoyama Y, Altered expression of chemokine receptor CXCR5 on T cells of myasthenia gravis patients. J. Neuroimmunol. 170, 172–178 (2005). [PubMed: 16214223]
20. Li X, Wu Z, Ding J, Zheng Z, Li X, Chen L, Zhu P, Role of the frequency of blood CD4+ CXCR5+ CCR6+T cells in autoimmunity in patients with Sjögren's syndrome. Biochem. Biophys. Res. Commun. 422, 238–244 (2012). [PubMed: 22575453]
21. Christensen JR, Börnsen L, Ratzer R, Piehl F, Khademi M, Olsson T, Sørensen PS, Sellebjerg F, Systemic inflammation in progressive multiple sclerosis involves follicular T-helper, Th17- and activated B-cells and correlates with progression. PLOS ONE 8, e57820 (2013). [PubMed: 23469245]
22. Ma J, Zhu C, Ma B, Tian J, Baidoo SE, Mao C, Wu W, Chen J, Tong J, Yang M, Jiao Z, Xu H, Lu L, Wang S, Increased frequency of circulating follicular helper T cells in patients with rheumatoid arthritis. Clin. Dev. Immunol. 2012, e827480 (2012).
23. Liu R, Wu Q, Su D, Che N, Chen H, Geng L, Chen J, Chen W, Li X, Sun L, A regulatory effect of IL-21 on T follicular helper-like cell and B cell in rheumatoid arthritis. Arthritis Res. Ther. 14, R255 (2012). [PubMed: 23176102]
24. Szabo K, Papp G, Barath S, Gyimesi E, Szanto A, Zeher M, Follicular helper T cells may play an important role in the severity of primary Sjögren's syndrome. Clin. Immunol. 147, 95–104 (2013). [PubMed: 23578551]
25. Kawamoto M, Harigai M, Hara M, Kawaguchi Y, Tezuka K, Tanaka M, Sugiura T, Katsumata Y, Fukasawa C, Ichida H, Higami S, Kamatani N, Expression and function of inducible co-stimulator in patients with systemic lupus erythematosus: Possible involvement in excessive interferon-gamma and anti-double-stranded DNA antibody production. Arthritis Res. Ther. 8, R62 (2006). [PubMed: 16563187]
26. Zhu C, Ma J, Liu Y, Tong J, Tian J, Chen J, Tang X, Xu H, Lu L, Wang S, Increased frequency of follicular helper T cells in patients with autoimmune thyroid disease. J. Clin. Endocrinol. Metab. 97, 943–950 (2012). [PubMed: 22188745]
27. Shan Y, Qi C, Zhao J, Liu Y, Gao H, Zhao D, Ding F, Wang J, Jiang Y, Higher frequency of peripheral blood follicular regulatory T cells in patients with new onset ankylosing spondylitis. Clin. Exp. Pharmacol. Physiol. 42, 154–161 (2015). [PubMed: 25345823]
28. Kim YU, Lim H, Jung HE, Wetsel RA, Chung Y, Regulation of autoimmune germinal center reactions in lupus-prone BXD2 mice by follicular helper T cells. PLOS ONE 10, (2015).
29. Wen Y, Yang B, Lu J, Zhang J, Yang H, Li J, Imbalance of circulating CD4+CXCR5+FOXP3+Tfr-like cells and CD4+CXCR5+FOXP3− Tfh-like cells in myasthenia gravis. Neurosci. Lett. 630, 176–182 (2016). [PubMed: 27473945]
30. Dhaeze T, Peelen E, Hombrouck A, Peeters L, Wijmeersch BV, Lemkens N, Lemkens P, Somers V, Lucas S, Broux B, Stinissen P, Hellings N, Circulating follicular regulatory t cells are defective in multiple sclerosis. J. Immunol 195, 832–840 (2015). [PubMed: 26071562]
31. Fonseca VR, Agua-Doce A, Maceiras AR, Pierson W, Ribeiro F, Romão VC, Pires AR, da Silva SL, Fonseca JE, Sousa AE, Linterman MA, Graca L, Human blood T_{fr} cells are indicators of

ongoing humoral activity not fully licensed with suppressive function. Sci. Immunol. 2, eaan1487 (2017). [PubMed: 28802258]

32. Linterman MA, Rigby RJ, Wong RK, Yu D, Brink R, Cannons JL, Schwartzberg PL, Cook MC, Walters GD, Vinuesa CG, Follicular helper T cells are required for systemic autoimmunity. J. Exp. Med. 206, 561–576 (2009). [PubMed: 19221396]
33. Vogel KU, Edelmann SL, Jeltsch KM, Bertossi A, Heger K, Heinz GA, Zöller J, Warth SC, Hoefig KP, Lohs C, Neff F, Kremmer E, Schick J, Repsilber D, Geerlof A, Blum H, Wurst W, Heikenwälder M, Schmidt-Supprian M, Heissmeyer V, Roquin paralogs 1 and 2 redundantly repress the Icos and Ox40 costimulator mRNAs and control follicular helper T cell differentiation. Immunity 38, 655–668 (2013). [PubMed: 23583643]
34. Di Y, Tan AH-M, Hu X, Athanasopoulos V, Simpson N, Silva DG, Hutloff A, Giles KM, Leedman PJ, Lam KP, Goodnow CC, Vinuesa CG, Roquin represses autoimmunity by limiting inducible T-cell co-stimulator messenger RNA. Nature 450, 299–303 (2007). [PubMed: 18172933]
35. Mino T, Murakawa Y, Fukao A, Vandenbon A, Wessels H-H, Ori D, Uehata T, Tartey S, Akira S, Suzuki Y, Vinuesa CG, Ohler U, Standley DM, Landthaler M, Fujiwara T, Takeuchi O, Regnase-1 and Roquin regulate a common element in inflammatory mRNAs by spatiotemporally distinct mechanisms. Cell 161, 1058–1073 (2015). [PubMed: 26000482]
36. Aloulou M, Carr EJ, Gador M, Bignon A, Liblau RS, Fazilleau N, Linterman MA, Follicular regulatory T cells can be specific for the immunizing antigen and derive from naive T cells. Nat. Commun. 7, 10579 (2016). [PubMed: 26818004]
37. Ritvo P-G, Saadawi A, Barennes P, Quiniou V, Chaara W, Soufi KE, Bonnet B, Six A, Shugay M, Mariotti-Ferrandiz E, Klatzmann D, High-resolution repertoire analysis reveals a major bystander activation of Tfh and Tfr cells. Proc. Natl. Acad. Sci. U.S.A. 115, 9604–9609 (2018). [PubMed: 30158170]
38. Maceiras AR, Almeida SCP, Mariotti-Ferrandiz E, Chaara W, Jebbawi F, Six A, Hori S, Klatzmann D, Faro J, Graca L, T follicular helper and T follicular regulatory cells have different TCR specificity. Nat. Commun. 8, 15067 (2017). [PubMed: 28429709]
39. Tafuri A, Shahinian A, Bladt F, Yoshinaga SK, Jordana M, Wakeham A, Boucher LM, Bouchard D, Chan VS, Duncan G, Odermatt B, Ho A, Itie A, Horan T, Whoriskey JS, Pawson T, Penninger JM, Ohashi PS, Mak TW, ICOS is essential for effective T-helper-cell responses. Nature 409, 105–109 (2001). [PubMed: 11343123]
40. Czar MJ, Kersh EN, Mijares LA, Lanier G, Lewis J, Yap G, Chen A, Sher A, Duckett CS, Ahmed R, Schwartzberg PL, Altered lymphocyte responses and cytokine production in mice deficient in the X-linked lymphoproliferative disease gene SH2D1A/DSHP/SAP. Proc. Natl. Acad. Sci. U.S.A. 98, 7449–7454 (2001). [PubMed: 11404475]
41. Choi YS, Kageyama R, Eto D, Escobar TC, Johnston RJ, Monticelli L, Lao C, Crotty S, ICOS receptor instructs T follicular helper cell versus effector cell differentiation via induction of the transcriptional repressor Bcl6. Immunity 34, 932–946 (2011). [PubMed: 21636296]
42. Qi H, Cannons JL, Klauschen F, Schwartzberg PL, Germain RN, SAP-controlled T-B cell interactions underlie germinal centre formation. Nature 455, 764–769 (2008). [PubMed: 18843362]
43. Cannons JL, Qi H, Lu KT, Dutta M, Gomez-Rodriguez J, Cheng J, Wakeland EK, Germain RN, Schwartzberg PL, Optimal germinal center responses require a multistage T cell:B cell adhesion process involving integrins, SLAM-associated protein, and CD84. Immunity 32, 253–265 (2010). [PubMed: 20153220]
44. Biram A, Winter E, Denton AE, Zaretsky I, Dassa B, Bemark M, Linterman MA, Yaari G, Shulman Z, B cell diversification is uncoupled from SAP-mediated selection forces in chronic germinal centers within Peyer's patches. Cell Rep. 30, 1910–1922.e5 (2020). [PubMed: 32049020]
45. Degn SE, van der Poel CE, Firl DJ, Ayoglu B, Al Qureshah FA, Bajic G, Mesin L, Reynaud C-A, Weill J-C, Utz PJ, Victora GD, Carroll MC, Clonal evolution of autoreactive germinal centers. Cell 170, 913–926.e19 (2017). [PubMed: 28841417]
46. Berland R, Fernandez L, Kari E, Han J-H, Lomakin I, Akira S, Wortis HH, Kearney JF, Ucci AA, Imanishi-Kari T, Toll-like receptor 7-dependent loss of B cell tolerance in pathogenic autoantibody knockin mice. Immunity 25, 429–440 (2006). [PubMed: 16973388]

47. Hollister K, Kusam S, Wu H, Clegg N, Mondal A, Sawant DV, Dent AL, Insights into the role of Bcl6 in follicular Th cells using a new conditional mutant mouse model. J. Immunol. 191, 3705–3711 (2013). [PubMed: 23980208]
48. Livet J, Weissman TA, Kang H, Draft RW, Lu J, Bennis RA, Sanes JR, Lichtman JW, Transgenic strategies for combinatorial expression of fluorescent proteins in the nervous system. Nature 450, 56–62 (2007). [PubMed: 17972876]
49. Tas JMJ, Mesin L, Pasqual G, Targ S, Jacobsen JT, Mano YM, Chen CS, Weill J-C, Reynaud C-A, Browne EP, Meyer-Hermann M, Victora GD, Visualizing antibody affinity maturation in germinal centers. Science 351, 1048–1054 (2016). [PubMed: 26912368]
50. Akama-Garren EH, van den Broek T, Simoni L, Castrillon C, van der Poel CE, Carroll MC, Follicular T cells are clonally and transcriptionally distinct in B cell-driven mouse autoimmune disease. Nat. Commun. 12, 6687 (2021). [PubMed: 34795279]
51. Lagattuta KA, Kang JB, Nathan A, Pauken KE, Jonsson AH, Rao DA, Sharpe AH, Ishigaki K, Raychaudhuri S, Repertoire analyses reveal T cell antigen receptor sequence features that influence T cell fate. Nat. Immunol. 23, 446–457 (2022). [PubMed: 35177831]
52. Burmeister Y, Lischke T, Dahler AC, Mages HW, Lam K-P, Coyle AJ, Kroczek RA, Hutloff A, ICOS controls the pool size of effector-memory and regulatory T cells. J. Immunol. 180, 774–782 (2008). [PubMed: 18178815]
53. Kisielow J, Obermair F-J, Kopf M, Deciphering $CD4^+$ T cell specificity using novel MHC–TCR chimeric receptors. Nat. Immunol. 20, 652–662 (2019). [PubMed: 30858620]
54. Joglekar AV, Li G, T cell antigen discovery. Nat. Methods 18, 873–880 (2021). [PubMed: 32632239]
55. Holst J, Szymczak-Workman AL, Vignali KM, Burton AR, Workman CJ, Vignali DAA, Generation of T-cell receptor retrogenic mice. Nat. Protoc. 1, 406–417 (2006). [PubMed: 17406263]
56. Castrillon C, Simoni L, van den Broek T, van der Poel C, Akama-Garren EH, Ma M, Carroll MC, Complex subsets but redundant clonality after B cells egress from spontaneous germinal centers. bioRxiv 2022.06.21.496939 [Preprint] (2022). 10.1101/2022.06.21.496939.
57. Nellore A, Zumaquero E, Scharer CD, Fucile CF, Tipton CM, King RG, Mi T, Mousseau B, Bradley JE, Zhou F, Mutneja S, Goepfert PA, Boss JM, Randall TD, Sanz I, Rosenberg AF, Lund FE, A transcriptionally distinct subset of influenza-specific effector memory B cells predicts long-lived antibody responses to vaccination in humans. Immunity 56, 847–863.e8 (2023). [PubMed: 36958335]
58. Tarca AL, Draghici S, Khatri P, Hassan SS, Mittal P, Kim J, Kim CJ, Kusanovic JP, Romero R, A novel signaling pathway impact analysis. Bioinformatics 25, 75–82 (2009). [PubMed: 18990722]
59. Tough DF, Borrow P, Sprent J, Induction of bystander T cell proliferation by viruses and type I interferon in vivo. Science 272, 1947–1950 (1996). [PubMed: 8658169]
60. Eberl G, Brawand P, MacDonald HR, Selective bystander proliferation of memory CD4+ and CD8+T cells upon NK T or T cell activation. J. Immunol. 165, 4305–4311 (2000). [PubMed: 11035065]
61. Mason D, A very high level of crossreactivity is an essential feature of the T-cell receptor. Immunol. Today 19, 395–404 (1998). [PubMed: 9745202]
62. Su LF, Kidd BA, Han A, Kotzin JJ, Davis MM, Virus-specific CD4+ memory-phenotype T cells are abundant in unexposed adults. Immunity 38, 373–383 (2013). [PubMed: 23395677]
63. Harkiolaki M, Holmes SL, Svendsen P, Gregersen JW, Jensen LT, McMahon R, Friese MA, van Boxel G, Etzensperger R, Tzartos JS, Kranc K, Sainsbury S, Harlos K, Mellins ED, Palace J, Esiri MM, van der Merwe PA, Jones EY, Fugger L, T cell-mediated autoimmune disease due to low-affinity crossreactivity to common microbial peptides. Immunity 30, 348–357 (2009). [PubMed: 19303388]
64. Lee V, Rodriguez DM, Ganci NK, Zeng S, Ai J, Chao JL, Walker MT, Miller CH, Klawon DEJ, Schoenbach MH, Kennedy DE, Maienschein-Cline M, Socci ND, Clark MR, Savage PA, The endogenous repertoire harbors self-reactive CD4+T cell clones that adopt a follicular helper T cell-like phenotype at steady state. Nat. Immunol. 24, 487–500 (2023). [PubMed: 36759711]

65. Viant C, Weymar GHJ, Escolano A, Chen S, Hartweger H, Cipolla M, Gazumyan A, Nussenzweig MC, Antibody affinity shapes the choice between memory and germinal center B cell fates. Cell 183, 1298–1311.e11 (2020). [PubMed: 33125897]
66. Nemazee D, Antigen receptor “capacity” and the sensitivity of self-tolerance. Immunol. Today 17, 25–29 (1996). [PubMed: 8652047]
67. Ochsenbein AF, Fehr T, Lutz C, Suter M, Brombacher F, Hengartner H, Zinkernagel RM, Control of early viral and bacterial distribution and disease by natural antibodies. Science 286, 2156–2159 (1999). [PubMed: 10591647]
68. Mazor RD, Nathan N, Gilboa A, Stoler-Barak L, Moss L, Solomonov I, Hanuna A, Divinsky Y, Shmueli MD, Hezroni H, Zaretsky I, Mor M, Golani O, Sabah G, Jakobson-Setton A, Yanichkin N, Feinmesser M, Tsoref D, Salman L, Yeoshoua E, Peretz E, Erlich I, Cohen NM, Gershoni JM, Freund N, Merbl Y, Yaari G, Eitan R, Sagi I, Shulman Z, Tumor-reactive antibodies evolve from non-binding and autoreactive precursors. Cell 185, 1208–1222.e21 (2022). [PubMed: 35305314]
69. Sangesland M, Torrents de la Peña A, Boyoglu-Barnum S, Ronsard L, Mohamed FAN, Moreno TB, Barnes RM, Rohrer D, Lonberg N, Ghebremichael M, Kanekiyo M, Ward A, Lingwood D, Allelic polymorphism controls autoreactivity and vaccine elicitation of human broadly neutralizing antibodies against influenza virus. Immunity 55, 1693–1709.e8 (2022). [PubMed: 35952670]
70. Elsner RA, Shlomchik MJ, Germinal center and extrafollicular B cell responses in vaccination, immunity, and autoimmunity. Immunity 53, 1136–1150 (2020). [PubMed: 33326765]
71. Odegard JM, Marks BR, DiPlacido LD, Poholek AC, Kono DH, Dong C, Flavell RA, Craft J, ICOS-dependent extrafollicular helper T cells elicit IgG production via IL-21 in systemic autoimmunity. J. Exp. Med. 205, 2873–2886 (2008). [PubMed: 18981236]
72. Sweet RA, Ols ML, Cullen JL, Milam AV, Yagita H, Shlomchik MJ, Facultative role for T cells in extrafollicular Toll-like receptor-dependent autoreactive B-cell responses in vivo. Proc. Natl. Acad. Sci. U.S.A. 108, 7932–7937 (2011). [PubMed: 21518858]
73. Jelcic I, Al Nimer F, Wang J, Lentsch V, Planas R, Jelcic I, Madjovski A, Ruhrmann S, Faigle W, Frauenknecht K, Pinilla C, Santos R, Hammer C, Ortiz Y, Opitz L, Grönlund H, Rogler G, Boyman O, Reynolds R, Lutterotti A, Khademi M, Olsson T, Piehl F, Sospedra M, Martin R, Memory B cells activate brain-homing, autoreactive CD4+T cells in multiple sclerosis. Cell 175, 85–100.e23 (2018). [PubMed: 30173916]
74. O’Neill SK, Shlomchik MJ, Glant TT, Cao Y, Doodes PD, Finnegan A, Antigen-specific B cells are required as APCs and autoantibody-producing cells for induction of severe autoimmune arthritis. J. Immunol. 174, 3781–3788 (2005). [PubMed: 15749919]
75. Clement RL, Daccache J, Mohammed MT, Diallo A, Blazar BR, Kuchroo VK, Lovitch SB, Sharpe AH, Sage PT, Follicular regulatory T cells control humoral and allergic immunity by restraining early B cell responses. Nat. Immunol. 20, 1360–1371 (2019). [PubMed: 31477921]
76. Cavazzoni CB, Hanson BL, Podestà MA, Bechu ED, Clement RL, Zhang H, Daccache J, Reyes-Robles T, Hett EC, Vora KA, Fadeyi OO, Oslund RC, Hazuda DJ, Sage PT, Follicular T cells optimize the germinal center response to SARS-CoV-2 protein vaccination in mice. Cell Rep. 38, 110399 (2022). [PubMed: 35139367]
77. Birnbaum ME, Mendoza JL, Sethi DK, Dong S, Glanville J, Dobbins J, Özkan E, Davis MM, Wucherpfennig KW, Garcia KC, Deconstructing the peptide-MHC specificity of T cell recognition. Cell 157, 1073–1087 (2014). [PubMed: 24855945]
78. Nelson RW, Beisang D, Tubo NJ, Dileepan T, Wiesner DL, Nielsen K, Wüthrich M, Klein BS, Kotov DI, Spanier JA, Fife BT, Moon JJ, Jenkins MK, T cell receptor Cross-reactivity between similar foreign and self peptides influences naive cell population size and autoimmunity. Immunity 42, 95–107 (2015). [PubMed: 25601203]
79. Liu GY, Fairchild PJ, Smith RM, Prowle JR, Kioussis D, Wraith DC, Low avidity recognition of self-antigen by T cells permits escape from central tolerance. Immunity 3, 407–415 (1995). [PubMed: 7584132]
80. Ellebrecht CT, Lundgren DK, Payne AS, On the mark: Genetically engineered immunotherapies for autoimmunity. Curr. Opin. Immunol. 61, 69–73 (2019). [PubMed: 31563849]

81. Ellebrecht CT, Bhoj VG, Nace A, Choi EJ, Mao X, Cho MJ, Di Zenzo G, Lanzavecchia A, Seykora JT, Cotsarelis G, Milone MC, Payne AS, Reengineering chimeric antigen receptor T cells for targeted therapy of autoimmune disease. Science 353, 179–184 (2016). [PubMed: 27365313]
82. Ferreira LMR, Muller YD, Bluestone JA, Tang Q, Next-generation regulatory T cell therapy. Nat. Rev. Drug Discov. 18, 749–769 (2019). [PubMed: 31541224]
83. Lanz TV, Brewer RC, Ho PP, Moon J-S, Jude KM, Fernandez D, Fernandes RA, Gomez AM, Nadj G-S, Bartley CM, Schubert RD, Hawes IA, Vazquez SE, Iyer M Zuchero JB, Teegen B, Dunn JE, Lock CB, Kipp LB, Cotham VC, Ueberheide BM, Aftab BT, Anderson MS, DeRisi JL, Wilson MR, Bashford-Rogers RJM, Platten M, Garcia KC, Steinman L, Robinson WH, Clonally expanded B cells in multiple sclerosis bind EBV EBNA1 and GlialCAM. Nature 603, 321–327 (2022). [PubMed: 35073561]
84. Serafini B, Rosicarelli B, Franciotta D, Magliozzi R, Reynolds R, Cinque P, Andreoni L, Trivedi P, Salvetti M, Faggioni A, Aloisi F, Dysregulated Epstein-Barr virus infection in the multiple sclerosis brain. J. Exp. Med. 204, 2899–2912 (2007). [PubMed: 17984305]
85. Bjornevik K, Cortese M, Healy BC, Kuhle J, Mina MJ, Leng Y, Elledge SJ, Niebuhr DW, Scher AI, Munger KL, Ascherio A, Longitudinal analysis reveals high prevalence of Epstein-Barr virus associated with multiple sclerosis. Science 375, 296–301 (2022). [PubMed: 35025605]
86. Lang HLE, Jacobsen H, Ikemizu S, Andersson C, Harlos K, Madsen L, Hjorth P, Sondergaard L, Svejgaard A, Wucherpfennig K, Stuart DI, Bell JI, Jones EY, Fugger L, A functional and structural basis for TCR cross-reactivity in multiple sclerosis. Nat. Immunol. 3, 940–943 (2002). [PubMed: 12244309]
87. Cui C, Wang J, Fagerberg E, Chen P-M, Connolly KA, Damo M, Cheung JF, Mao T, Askari AS, Chen S, Fitzgerald B, Foster GG, Eisenbarth SC, Zhao H, Craft J, Joshi NS, Neoantigen-driven B cell and CD4 T follicular helper cell collaboration promotes anti-tumor CD8 T cell responses. Cell 184, 6101–6118.e13 (2021). [PubMed: 34852236]
88. Zander R, Kasmani MY, Chen Y, Topchyan P, Shen J, Zheng S, Burns R, Ingram J, Cui C, Joshi N, Craft J, Zajac A, Cui W, Tfh-cell-derived interleukin 21 sustains effector CD8+T cell responses during chronic viral infection. Immunity 55, 475–493.e5 (2022). [PubMed: 35216666]
89. Zander R, Schauder D, Xin G, Nguyen C, Wu X, Zajac A, Cui W, CD4+T cell help is required for the formation of a cytolytic CD8+T cell subset that protects against chronic infection and cancer. Immunity 51, 1028–1042.e4 (2019). [PubMed: 31810883]
90. Woodruff MC, Ramonell RP, Nguyen DC, Cashman KS, Saini AS, Haddad NS, Ley AM, Kyu S, Howell JC, Ozturk T, Lee S, Suryadevara N, Case JB, Bugrovsky R, Chen W, Estrada J, Morrison-Porter A, Derrico A, Anam FA, Sharma M, Wu HM, Le SN, Jenks SA, Tipton CM, Staitieh B, Daiss JL, Ghosn E, Diamond MS, Carnahan RH, Crowe JE, Hu WT, Lee FE-H, Sanz I, Extrafollicular B cell responses correlate with neutralizing antibodies and morbidity in COVID-19. Nat. Immunol. 21, 1506–1516 (2020). [PubMed: 33028979]
91. Bastard P, Rosen LB, Zhang Q, Michailidis E, Hoffmann H-H, Zhang Y, Dorgham K, Philippot Q, Rosain J, Béziat V, Manry J, Shaw E, Haljasmägi L, Peterson P, Lorenzo L, Bizien L, Trouillet-Assant S, Dobbs K, de Jesus AA, Belot A, Kallaste A, Catherinot E, Tandjaoui-Lambiotte Y, Le Pen J, Kerner G, Bigio B, Seeleuthner Y, Yang R, Bolze A, Spaan AN, Delmonte OM, Abers MS, Aiuti A, Casari G, Lampasona V, Piemonti L, Ciceri F, Bilguvar K, Lifton RP, Vasse M, Smadja DM, Migaud M, Hadjadj J, Terrier B, Duffy D, Quintana-Murci L, van de Beek D, Roussel L, Vinh DC, Tangye SG, Haerynck F, Dalmau D, Martinez-Picado J, Brodin P, Nussenzweig MC, Boisson-Dupuis S, Rodríguez-Gallego C, Vogt G, Mogensen TH, Oler AJ, Gu J, Burbelo PD, Cohen JI, Biondi A, Bettini LR, D'Angio M, Bonfanti P, Rossignol P, Mayaux J, Rieux-Laucat F, Husebye ES, Fusco F, Ursini MV, Imberti L, Sottini A, Paghera S, Quiros-Roldan E, Rossi C, Castagnoli R, Montagna D, Licari A, Marseglia GL, Duval X, Ghosn J, HGID Lab; NIAID-USUHS Immune Response to COVID Group, COVID Clinicians; COVID-STORM Clinicians, Imagine COVID Group; French COVID Cohort Study Group, Milieu Intérieur Consortium; CoV-Contact Cohort, Amsterdam UMC Covid-19 Biobank, COVID Human Genetic Effort, Tsang JS, Goldbach-Mansky R, Kisand K, Lionakis MS, Puel A, Zhang S-Y, Holland SM, Gorochov G, Jouanguy E, Rice CM, Cobat A, Notarangelo LD, Abel L, Su HC, Casanova J-L, Autoantibodies against type I IFNs in patients with life-threatening COVID-19. Science 370, eabd4585 (2020). [PubMed: 32972996]

92. Wang EY, Mao T, Klein J, Dai Y, Huck JD, Jaycox JR, Liu F, Zhou T, Israelow B, Wong P, Coppi A, Lucas C, Silva J, Oh JE, Song E, Perotti ES, Zheng NS, Fischer S, Campbell M, Fournier JB, Wyllie AL, Vogels CBF, Ott IM, Kalinich CC, Petrone ME, Watkins AE, Dela Cruz C, Farhadian SF, Schulz WL, Ma S, Grubaugh ND, Ko AI, Iwasaki A, Ring AM, Diverse functional autoantibodies in patients with COVID-19. Nature 595, 283–288 (2021). [PubMed: 34010947]

93. Chang SE, Feng A, Meng W, Apostolidis SA, Mack E, Artandi M, Barman L, Bennett K, Chakraborty S, Chang I, Cheung P, Chinthrajah S, Dhingra S, Do E, Finck A, Gaano A, Geßner R, Giannini HM, Gonzalez J, Greib S, Gündisch M, Hsu AR, Kuo A, Manohar M, Mao R, Neeli I, Neubauer A, Oniyide O, Powell AE, Puri R, Renz H, Schapiro J, Weidenbacher PA, Wittman R, Ahuja N, Chung H-R, Jagannathan P, James JA, Kim PS, Meyer NJ, Nadeau KC, Radic M, Robinson WH, Singh U, Wang TT, Wherry EJ, Skevaki C, Prak ETL, Utz PJ, New-onset IgG autoantibodies in hospitalized patients with COVID-19. Nat. Commun. 12, 5417 (2021). [PubMed: 34521836]

94. Gruber CN, Patel RS, Trachtman R, Lepow L, Amanat F, Krammer F, Wilson KM, Onel K, Geanon D, Tuballes K, Patel M, Mouskas K, O'Donnell T, Merritt E, Simons NW, Barcessat V, Valle DMD, Udondem S, Kang G, Gangadharan S, Ofori-Amanfo G, Laserson U, Rahman A, Kim-Schulze S, Charney AW, Gnjatic S, Gelb BD, Merad M, Bogunovic D, Mapping systemic inflammation and antibody responses in multisystem inflammatory syndrome in children (MIS-C). Cell 183, 982–995.e14 (2020). [PubMed: 32991843]

95. Zuo Y, Estes SK, Ali RA, Gandhi AA, Yalavarthi S, Shi H, Sule G, Gockman K, Madison JA, Zuo M, Yadav V, Wang J, Woodard W, Lezak SP, Lugogo NL, Smith SA, Morrissey JH, Kanthi Y, Knight JS, Prothrombotic autoantibodies in serum from patients hospitalized with COVID-19. Sci. Transl. Med. 12, eabd3876 (2020). [PubMed: 33139519]

96. Su Y, Yuan D, Chen DG, Ng RH, Wang K, Choi J, Li S, Hong S, Zhang R, Xie J, Kornilov SA, Scherler K, Pavlovitch-Bedzyk AJ, Dong S, Lausted C, Lee I, Fallen S, Dai CL, Baloni P, Smith B, Duvvuri VR, Anderson KG, Li J, Yang F, Duncombe CJ, McCulloch DJ, Rostomily C, Troisch P, Zhou J, Mackay S, DeGottardi Q, May DH, Taniguchi R, Gittelman RM, Klinger M, Snyder TM, Roper R, Wojciechowska G, Murray K, Edmark R, Evans S, Jones L, Zhou Y, Rowen L, Liu R, Chour W, Algren HA, Berrington WR, Wallick JA, Cochran RA, Micikas ME, the ISB-Swedish COVID-19 Biobanking Unit, Wrin T, Petropoulos CJ, Cole HR, Fischer TD, Wei W, Hoon DSB, Price ND, Subramanian N, Hill JA, Hadlock J, Magis AT, Ribas A, Lanier LL, Boyd SD, Bluestone JA, Chu H, Hood L, Gottardo R, Greenberg PD, Davis MM, Goldman JD, Heath JR, Multiple early factors anticipate post-acute COVID-19 sequelae. Cell 185, 881–895.e20 (2022). [PubMed: 35216672]

97. Shulman Z, Gitlin AD, Targ S, Jankovic M, Pasqual G, Nussenzweig MC, Victora GD, T follicular helper cell dynamics in germinal centers. Science 341, 673–677 (2013). [PubMed: 23887872]

98. Letourneur F, Malissen B, Derivation of a T cell hybridoma variant deprived of functional T cell receptor alpha and beta chain transcripts reveals a nonfunctional alpha-mRNA of BW5147 origin. Eur. J. Immunol. 19, 2269–2274 (1989). [PubMed: 2558022]

99. Kingston RE, Chen CA, Rose JK, Calcium phosphate transfection. Curr. Protoc. Mol. Biol. 63, 9.1.1–9.1.11 (2003).

100. Akama-Garren EH, Joshi NS, Tammela T, Chang GP, Wagner BL, Lee D-Y, Rideout WM, Papagiannakopoulos T, Xue W, Jacks T, A modular assembly platform for rapid generation of DNA constructs. Sci. Rep. 6, 16836 (2016). [PubMed: 26887506]

101. Gong S, Kus L, Heintz N, Rapid bacterial artificial chromosome modification for large-scale mouse transgenesis. Nat. Protoc. 5, 1678–1696 (2010). [PubMed: 20885380]

102. Singh U, Wurtele ES, orfipy: A fast and flexible tool for extracting ORFs. Bioinformatics 37, 3019–3020 (2021). [PubMed: 33576786]

103. Reynisson B, Alvarez B, Paul S, Peters B, Nielsen M, NetMHCpan-4.1 and NetMHCIIpan-4.0: Improved predictions of MHC antigen presentation by concurrent motif deconvolution and integration of MS MHC eluted ligand data. Nucleic Acids Res. 48, W449–W454 (2020). [PubMed: 32406916]

104. Ayoglu B, Mitsios N, Kockum I, Khademi M, Zandian A, Sjöberg R, Forsström B, Bredenberg J, Lima Bomfim I, Holmgren E, Grönlund H, Guerreiro-Cacais AO, Abdelmagid N, Uhlén M, Waterboer T, Alfredsson L, Mulder J, Schwenk JM, Olsson T, Nilsson P, Anoctamin 2 identified

as an autoimmune target in multiple sclerosis. Proc. Natl. Acad. Sci. U.S.A. 113, 2188–2193 (2016). [PubMed: 26862169]

105. Hao Y, Hao S, Andersen-Nissen E, Mauck WM, Zheng S, Butler A, Lee MJ, Wilk AJ, Darby C, Zager M, Hoffman P, Stoeckius M, Papalexi E, Mimitou EP, Jain J, Srivastava A, Stuart T, Fleming LM, Yeung B, Rogers AJ, McElrath JM, Blish CA, Gottardo R, Smibert P, Satija R, Integrated analysis of multimodal single-cell data. Cell 184, 3573–3587.e29 (2021). [PubMed: 34062119]
106. Korsunsky I, Millard N, Fan J, Slowikowski K, Zhang F, Wei K, Baglaenko Y, Brenner M, Loh P, Raychaudhuri S, Fast, sensitive and accurate integration of single-cell data with Harmony. Nat. Methods 16, 1289–1296 (2019). [PubMed: 31740819]
107. Finak G, McDavid A, Yajima M, Deng J, Gersuk V, Shalek AK, Slichter CK, Miller HW, McElrath MJ, Prlic M, Linsley PS, Gottardo R, MAST: A flexible statistical framework for assessing transcriptional changes and characterizing heterogeneity in single-cell RNA sequencing data. Genome Biol. 16, 278 (2015). [PubMed: 26653891]
108. Yu G, Wang L-G, Han Y, He Q-Y, clusterProfiler: An R package for comparing biological themes among gene clusters. OMICS 16, 284–287 (2012). [PubMed: 22455463]
109. Ashburner M, Ball CA, Blake JA, Botstein D, Butler H, Cherry JM, Davis AP, Dolinski K, Dwight SS, Eppig JT, Harris MA, Hill DP, Issel-Tarver L, Kasarskis A, Lewis S, Matese JC, Richardson JE, Ringwald M, Rubin GM, Sherlock G, Gene Ontology: Tool for the unification of biology. Nat. Genet. 25, 25–29 (2000). [PubMed: 10802651]
110. The Gene Ontology Consortium, The gene ontology resource: 20 years and still GOing strong. Nucleic Acids Res. 47, D330–D338 (2019). [PubMed: 30395331]
111. Subramanian A, Tamayo P, Mootha VK, Mukherjee S, Ebert BL, Gillette MA, Paulovich A, Pomeroy SL, Golub TR, Lander ES, Mesirov JP, Gene set enrichment analysis: A knowledge-based approach for interpreting genome-wide expression profiles. Proc. Natl. Acad. Sci. U.S.A. 102, 15545–15550 (2005). [PubMed: 16199517]
112. Liberzon A, Subramanian A, Pinchback R, Thorvaldsdóttir H, Tamayo P, Mesirov JP, Molecular signatures database (MSigDB) 3.0. Bioinformatics 27, 1739–1740 (2011). [PubMed: 21546393]
113. Schnell A, Huang L, Singer M, Singaraju A, Barilla RM, Regan BML, Bollhagen A, Thakore PI, Dionne D, Delorey TM, Pawlak M, Horste GMZ, Rozenblatt-Rosen O, Irizarry RA, Regev A, Kuchroo VK, Stem-like intestinal Th17 cells give rise to pathogenic effector T cells during autoimmunity. Cell 184, 6281–6298.e23 (2021). [PubMed: 34875227]
114. Huang H, Wang C, Rubelt F, Scriba TJ, Davis MM, Analyzing the Mycobacterium tuberculosis immune response by T-cell receptor clustering with GLIPH2 and genome-wide antigen screening. Nat. Biotechnol. 38, 1194–1202 (2020). [PubMed: 32341563]
115. Zhang H, Zhan X, Li B, GIANA allows computationally-efficient TCR clustering and multi-disease repertoire classification by isometric transformation. Nat. Commun. 12, 4699 (2021). [PubMed: 34349111]
116. Mayer-Blackwell K, Schattgen S, Cohen-Lavi L, Crawford JC, Souquette A, Gaevert JA, Hertz T, Thomas PG, Bradley P, Fiore-Gartland A, TCR meta-clonotypes for biomarker discovery with tcrdist3 enabled identification of public, HLA-restricted clusters of SARS-CoV-2 TCRs. eLife 10, e68605 (2021). [PubMed: 34845983]
117. Sethna Z, Elhanati Y, Callan CG, Walczak AM, Mora T, OLGA: Fast computation of generation probabilities of B- and T-cell receptor amino acid sequences and motifs. Bioinformatics 35, 2974–2981 (2019). [PubMed: 30657870]
118. Sidhom J-W, Larman HB, Pardoll DM, Baras AS, DeepTCR is a deep learning framework for revealing sequence concepts within T-cell repertoires. Nat. Commun. 12, 1605 (2021). [PubMed: 33707415]
119. Evans R, O'Neill M, Pritzel A, Antropova N, Senior A, Green T, Žídek A, Bates R, Blackwell S, Yim J, Ronneberger O, Bodenstein S, Zielinski M, Bridgland A, Potapenko A, Cowie A, Tunyasuvunakool K, Jain R, Clancy E, Kohli P, Jumper J, Hassabis D, Protein complex prediction with AlphaFold-Multimer. bioRxiv 2021.10.04.463034 [Preprint] (2022). 10.1101/2021.10.04.463034.

120. Stirling DR, Swain-Bowden MJ, Lucas AM, Carpenter AE, Cimini BA, Goodman A, CellProfiler 4: Improvements in speed, utility and usability. BMC Bioinformatics 22, 433 (2021). [PubMed: 34507520]

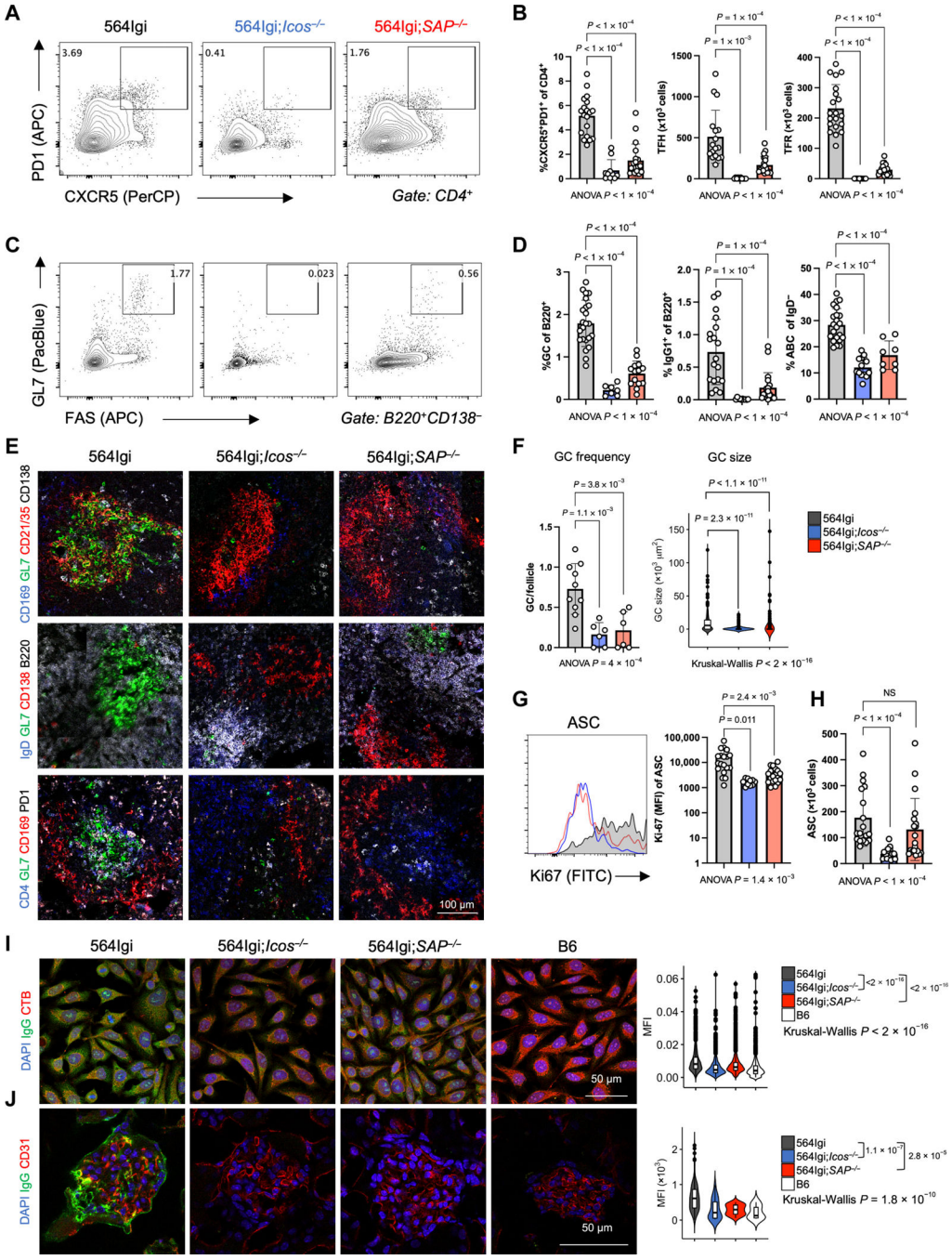

Fig. 1. Autoreactive GC formation is T cell dependent.

(**A** and **B**) Flow cytometry contour plots (A) and quantification (B) of follicular T cell frequency in the spleens of 10-week-old 564igi ($n = 23$), 564igi;*Icos*$^{-/-}$ ($n = 7$), or 564igi;*SAP*$^{-/-}$ ($n = 14$) mice. (**C** and **D**) Flow cytometry contour plots (c) and quantification (D) of GC (GL7$^+$FAS$^+$), IgG1$^+$ B cell, and ABC (CD11c$^+$CD21/35$^-$ of B220$^+$CD138$^-$GL7$^-$CD38$^+$IgD$^-$) frequency in the spleens of 10-week-old 564Igi, 564Igi;*Icos*$^{-/-}$, or 564Igi;*SAP*$^{-/-}$ mice. (**E**) Confocal microscopy of spleens stained for

indicated markers from 10-week-old 564Igi (n = 10), 564Igi;*Icos*$^{-/-}$ (n = 6), or 564Igi;*SAP*$^{-/-}$ (n = 6) mice. (**F**) Quantification of average number of GCs per follicle per mouse (left) or GC size (right) from confocal staining in (E). (**G**) Flow cytometry histogram (left) and quantification (right) of Ki67 expression in ASCs (CD138^{+}) in the spleens of 10-week-old 564Igi, 564Igi;*Icos*$^{-/-}$, or 564Igi;*SAP*$^{-/-}$ mice. Fitc, fluorescein isothiocyanate. (**H**) Bar plot of flow cytometric quantification of total number of ASCs in the spleens of 10-week-old 564Igi, 564Igi;*Icos*$^{-/-}$, or 564Igi;*SAP*$^{-/-}$ mice. nS, not significant. (**I**) Confocal microscopy (left) and quantification of nuclear IgG staining (right) of HEp-2 cells incubated with sera from 10-week-old 564Igi (n = 5), 564Igi;*Icos*$^{-/-}$ (n = 4), 564Igi;*SAP*$^{-/-}$ (n = 4), or B6 (n = 3) mice. (**J**) Confocal microscopy (left) and quantification of glomerular IgG deposition (right) in kidneys from 564Igi (n = 3), 564Igi;*Icos*$^{-/-}$ (n = 3), 564Igi;*SAP*$^{-/-}$ (n = 3), or B6 (n = 3) mice. Data are representative of three independent experiments. Data are represented as means ± SD. P value was computed using two-tailed Student's t test for two-way comparisons or AnoVA or Kruskal-Wallis for grouped comparisons.

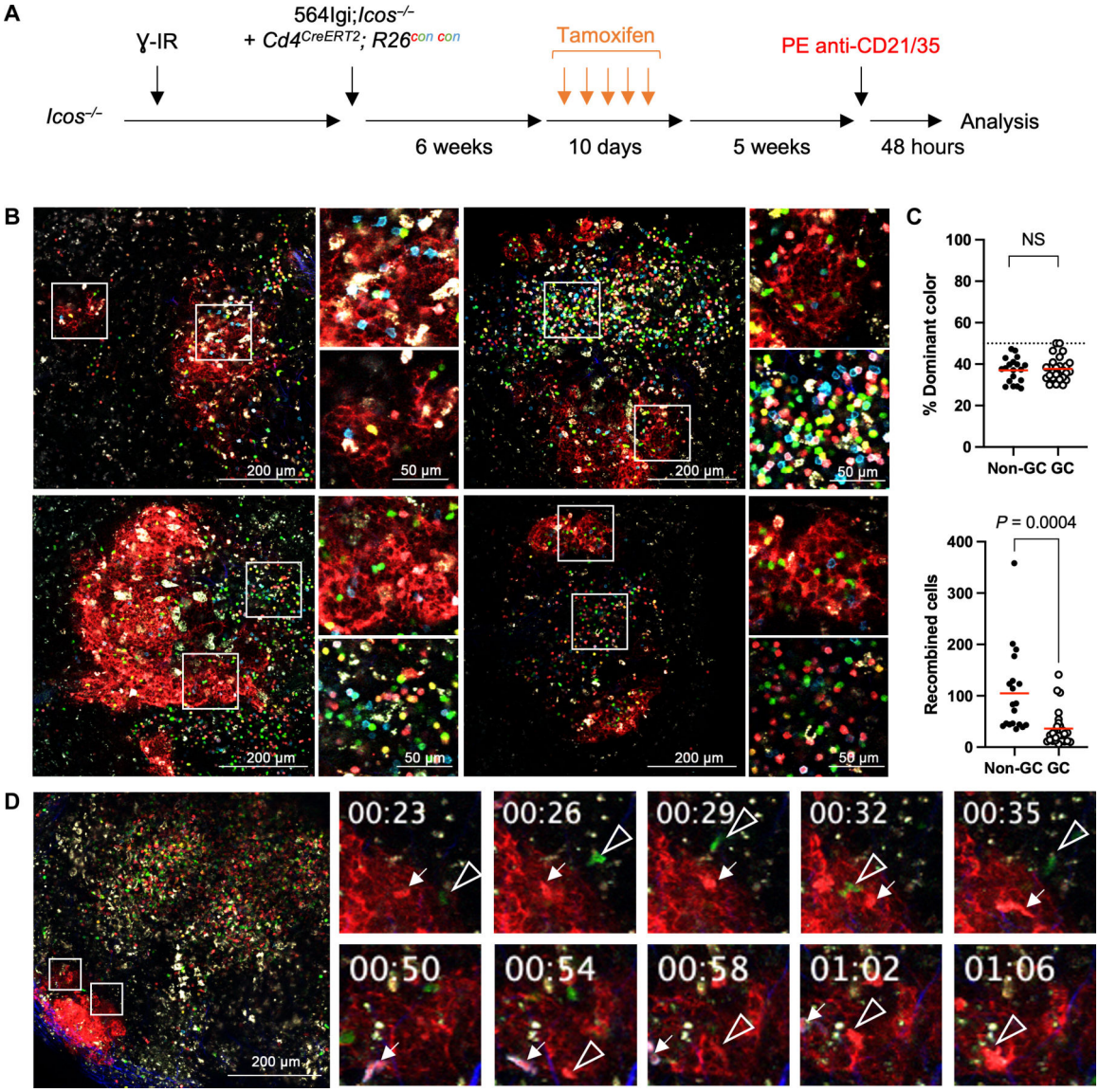

Fig. 2. Follicular T cells are polyclonal and dynamic.

(**A**) Experimental diagram. *Icos*$^{-/-}$ mice were lethally irradiated with 11 Gy, followed by intravenous reconstitution with a mix of 1p 564Igi;*Icos*$^{-/-}$ and 2p *Cd4*^{CreERT2};*R26*$^{con/con}$ bone marrow. Six weeks after irradiation, mixed bone marrow chimeras were treated with five doses of tamoxifen (50 mg/kg, intraperitoneally) every 2 days. Five weeks after tamoxifen treatment, bone marrow chimeras were injected intravenously with 3 μg of PE anti-cD21/35 to label FDCs. Two days later, mice were analyzed by intravital multiphoton microscopy. (**B**) Multiphoton microscopy of spleens from autoimmune bone marrow chimeras (n = 15). insets (right) show higher magnification of non-GC or GC resident T cell populations. (**C**) Quantification of CD4 clonality (top) or number of recombined cells (bottom) from (B). horizontal line indicates 50% dominance. GC was determined by CD21/35 staining. Red line indicates mean. P value computed using two-tailed Student's t test. (**D**) Intravital multiphoton microscopy of inguinal lymph node of an autoimmune bone

marrow chimera. Arrows track individual follicular T cell clones entering and leaving a GC. Time is represented as HH:MM. Data are representative of three independent experiments.

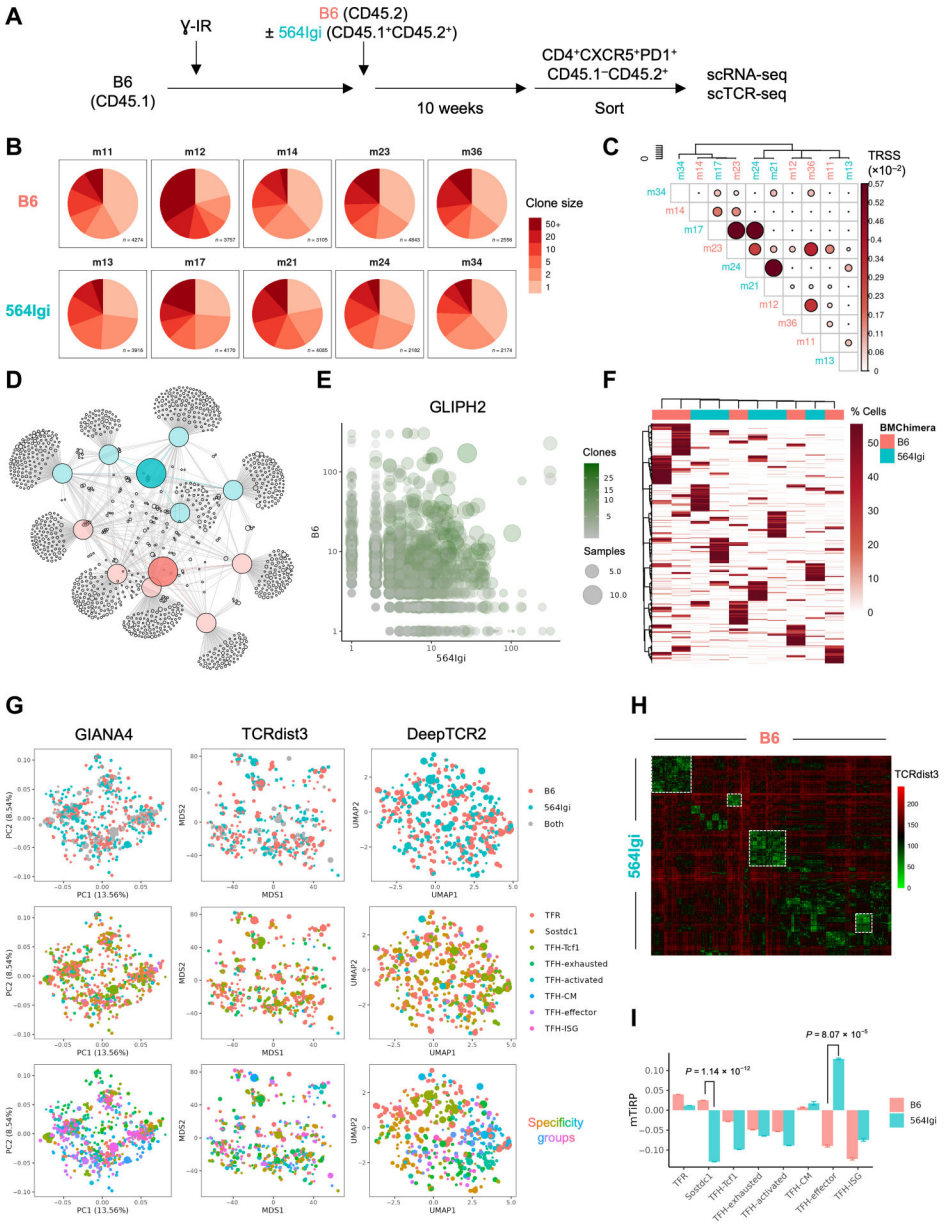

Fig. 3. Autoimmune and foreign antigen follicular T cell repertoires share predicted specificities.

(**A**) experimental diagram. B6 (cD45.1) mice were lethally irradiated with 11 Gy, followed by intravenous reconstitution with a mix of 1p 564Igi (cD45.1^{+}cD45.2^{+}) and 2p B6 (cD45.2) bone marrow. ten weeks after irradiation, follicular T cells (cD4^{+}cXcR5^{+}PD1^{+}cD45.1^{-}cD45.2^{+}) were sorted from the spleens of autoimmune bone marrow chimeras (564Igi; $n = 5$) or NPOVA–immunized controls (B6; $n = 5$) and analyzed by scRNA-seq and scTCR-seq. (**B**) Pie charts of clonal expansion of follicular t cells in individual bone marrow chimeras. Pie slice size represents proportion of cells in clones (defined by cDR3αβ) of indicated size. number of cells is shown in bottom right. (**C**) Symmetric correlation plot of TRSSs between cDR3αβ repertoires of individual bone marrow chimeras. Sample names are colored according to experimental group (B6, red; 564Igi, blue). (**D**) unweighted network plot of expanded (greater than five cells) clones (defined by cDR3β).

colored points represent individual samples (B6, red; 564Igi, blue), edges indicate clone presence in each repertoire, and size represents number of cells in each clone. (**E**) Scatter plot comparing GLIPH2 group size between immunized (B6) and autoimmune (564Igi) bone marrow chimeras. Specificity groups are colored according to the number of unique clones (defined by cDR3αβ) that belong to a given GLIPH2 group and sized according to number of bone marrow chimeras in which the given specificity group is observed. (**F**) hierarchical heatmap of GLIPH2 sharing across individual samples. columns represent bone marrow chimeras, and rows represent GLIPH2 groups. (**G**) Dimensionality reduction plots of different methods of computational prediction of TCR similarity (columns) colored according to treatment group, scRNA-seq assigned cluster, or *k*–nearest neighbor clustering assigned specificity group (metaclonotypes). individual clonotypes are depicted as circles and sized according to number of cells in each clonotype. GIANA4 dimensionality reduction calculated using isometric encoding of amino acid sequences of clones (defined by cDR3β). TCRdist3 dimensionality reduction calculated using pairwise TCR distance calculations between clones (defined by TCRβ). DeepTCR2 dimensionality reduction calculated using VAE-based unsupervised sequence featurization of clones (defined by TCRαβ). PC, principal component. (**H**) hierarchical heatmap of TCRdist3 comparison scores between each clone (defined by TCRβ) in the B6 repertoire (columns) and each clone in the 564ligi repertoire (rows). Groups of closely related clones highlighted in white boxes. (**I**) mTiRP calculated from scTCR-seq data of follicular T cell repertoires from immunized (B6, red) or autoimmune (564lgi, blue) bone marrow chimeras. Data are representative of three independent experiments.

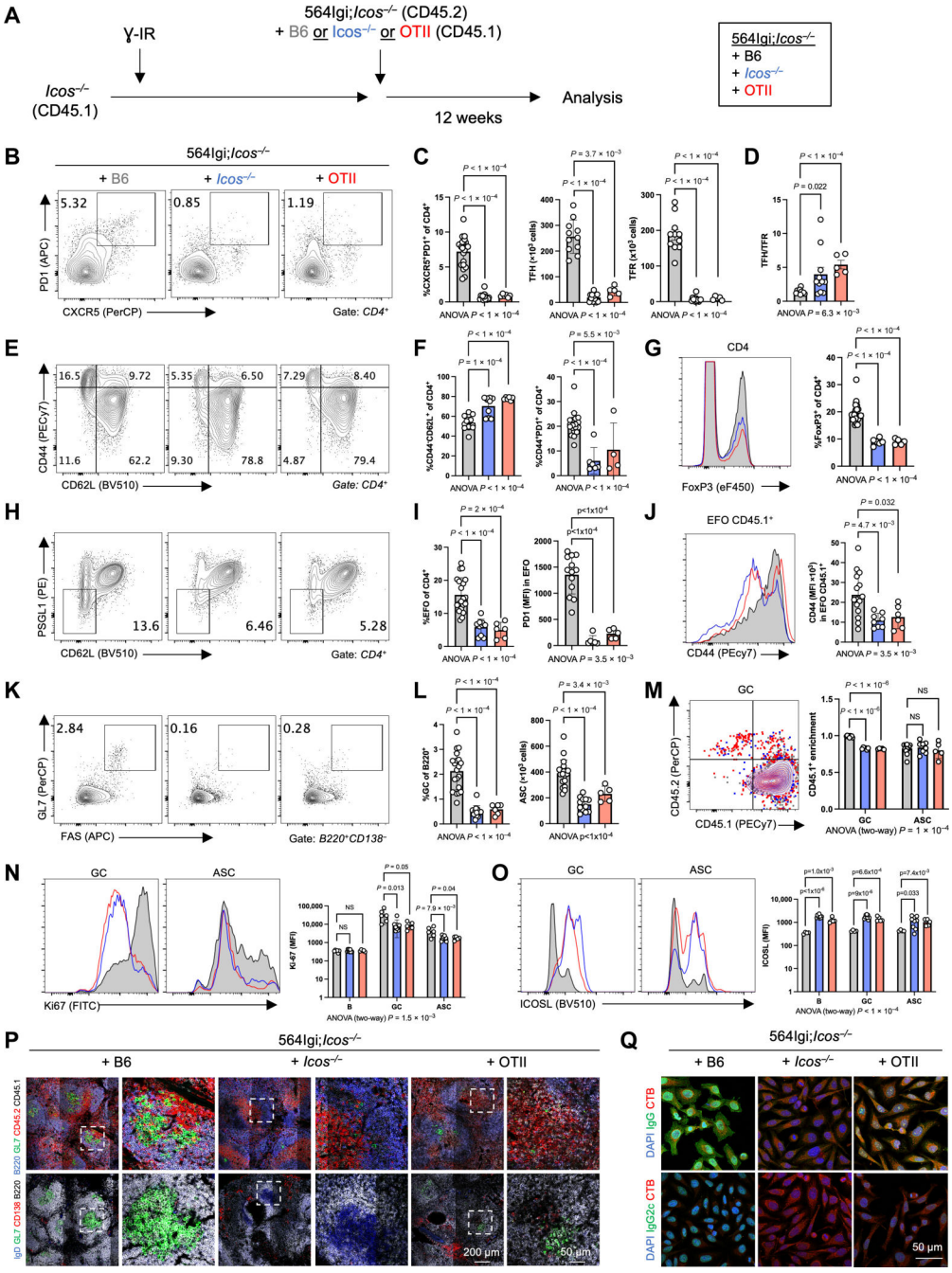

Fig. 4. Follicular T cell initiation of autoreactive GCs is TCR dependent.

(**A**) Experimental diagram. *Icos*$^{-/-}$ (cD45.1) mice were lethally irradiated with 11 Gy, followed by intravenous reconstitution with a mix of 1p 564Igi;*Icos*$^{-/-}$ (CD45.2) and 2p B6, *Icos*$^{-/-}$, or OTII (CD45.1) bone marrow. Twelve weeks after irradiation, mixed bone marrow chimeras were analyzed by flow cytometry. (**B** and **C**) Flow cytometry contour plots (B) and quantification (C) of follicular T cell frequency in the spleens of B6 (n = 20), *Icos*$^{-/-}$ (n = 13), or OTII (n = 6) mixed autoimmune chimeras. (**D**) Bar plot of the ratio of T_{Fh} ($CD4^+CXCR5^+PD1^+FoxP3^-$) to TT_{FR} ($CD4^+CXCR5^+PD1^+FoxP3^+$) cells. (**E**

and **F**) Flow cytometry contour plots (E) and quantification (F) of naïve and activated CD4 T cell frequency. (**G**) Flow cytometry histogram (left) and quantification (right) of FoxP3 expression in CD4 t cells. (**H** and **I**) Flow cytometry contour plots (E) and quantification (F) of EFO ($PSGl1^{-}cD62l^{-}$) CD4 T cell frequency and PD1 expression in EFO cells. (**J**) Flow cytometry histogram (left) and quantification (right) of CD44 expression in $CD45.1^{+}$ EFO cells. (**K** and **L**) Flow cytometry contour plots (K) and quantification (L) of GC B cell frequency and ASC ($CD138^{+}$) number. (**M**) overlaid flow cytometry contour plot (left) and quantification (right) of non-564Igi derived ($CD45.1^{+}CD45.2^{-}$) GC B cells or ASCs in B6 (gray), $Icos^{-/-}$ (blue), or OTII (red) mixed autoimmune chimeras. Enrichment represents $CD45.1^{+}CD45.2^{-}$ frequency in indicated population relative to $CD45.1^{+}CD45.2^{-}$ frequency in follicular B cells. (**N**) Flow cytometry histograms (left) and quantification (right) of Ki67 expression in GC B cells and ASCs. (**O**) Flow cytometry histograms (left) and quantification (right) of ICOSL expression in GC B cells and ASCs. (**P** and **Q**) Confocal microscopy of spleens from B6 ($n = 3$), $Icos^{-/-}$ ($n = 3$), or OTII ($n = 3$) mixed autoimmune chimeras (P) or HEp-2 cells (Q) stained for indicated markers. insets (right) show higher magnification. Data are representative of four independent experiments. Data are represented as means ± SD. *P* value was computed using two-tailed Student's *t* test for two-w ay comparisons or two-way ANOVA for grouped comparisons.

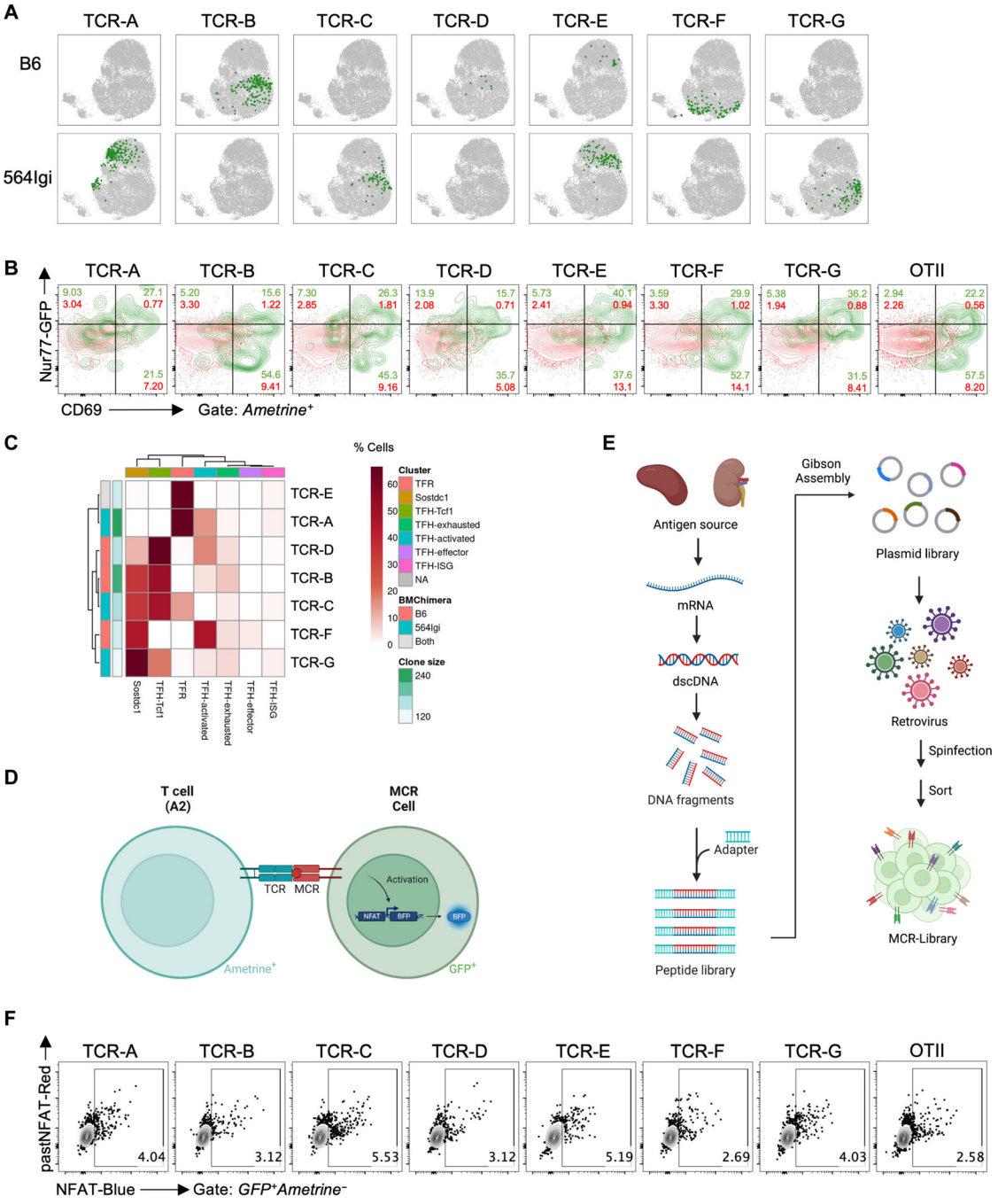

Fig. 5. Construction of an autoantigen library for cognate CD4 TCR peptide identification.

(**A**) mappings of seven orphan clonotypes from immunized (B6, top) or autoimmune (564lgi, bottom) bone marrow chimeras onto UMAP visualization of scRNA-seq data from Fig. 3A. (**B**) Overlaid flow cytometry contour plots of Nur77-GFP reporter activation and CD69 expression after 24-hour coculture of TCR hybridomas expressing each orphan TCR with 564lgi splenocytes (green) or no stimulation (red). (**C**) Hierarchical heatmap of sharing of candidate TCRs from (A) across assigned clusters. Columns represent clusters, and rows represent clones, colored according to their presence in either B6 (red), 564igi (blue), or

both (gray) repertoires and sizes. (**D**) Experimental schematic of MCR coculture system. TCR-Expressing hybridomas (Ametrine^{+}) are cocultured with NFAT reporter cells (GFP^{+}) expressing an MHC class II extracellular domain covalently linked to candidate peptides and an intracellular TCR signaling domain. Cognate antigen recognition results in reporter activation of MCR cells, which may be enriched through iterative sorting. Created with BioRender.com. (**E**) Experimental schematic of MCR library construction. The spleen and kidney were used as autoantigen sources to generate dscDNA. After random fragmentation and adapter ligation, peptide sequences were cloned into the MCR vector by Gibson Assembly. the peptide library was retrovirally transduced into nFAt reporter cells and sorted for mhc class ii expression, generating a transcriptome-wide library of autoantigen peptides. created with BioRender.com. (**F**) Flow cytometry contour plots of NFAT reporter activation in cells expressing a transcriptome-wide library of autoantigen peptides (MCR-Lib) after coculture with indicated orphan TCR.

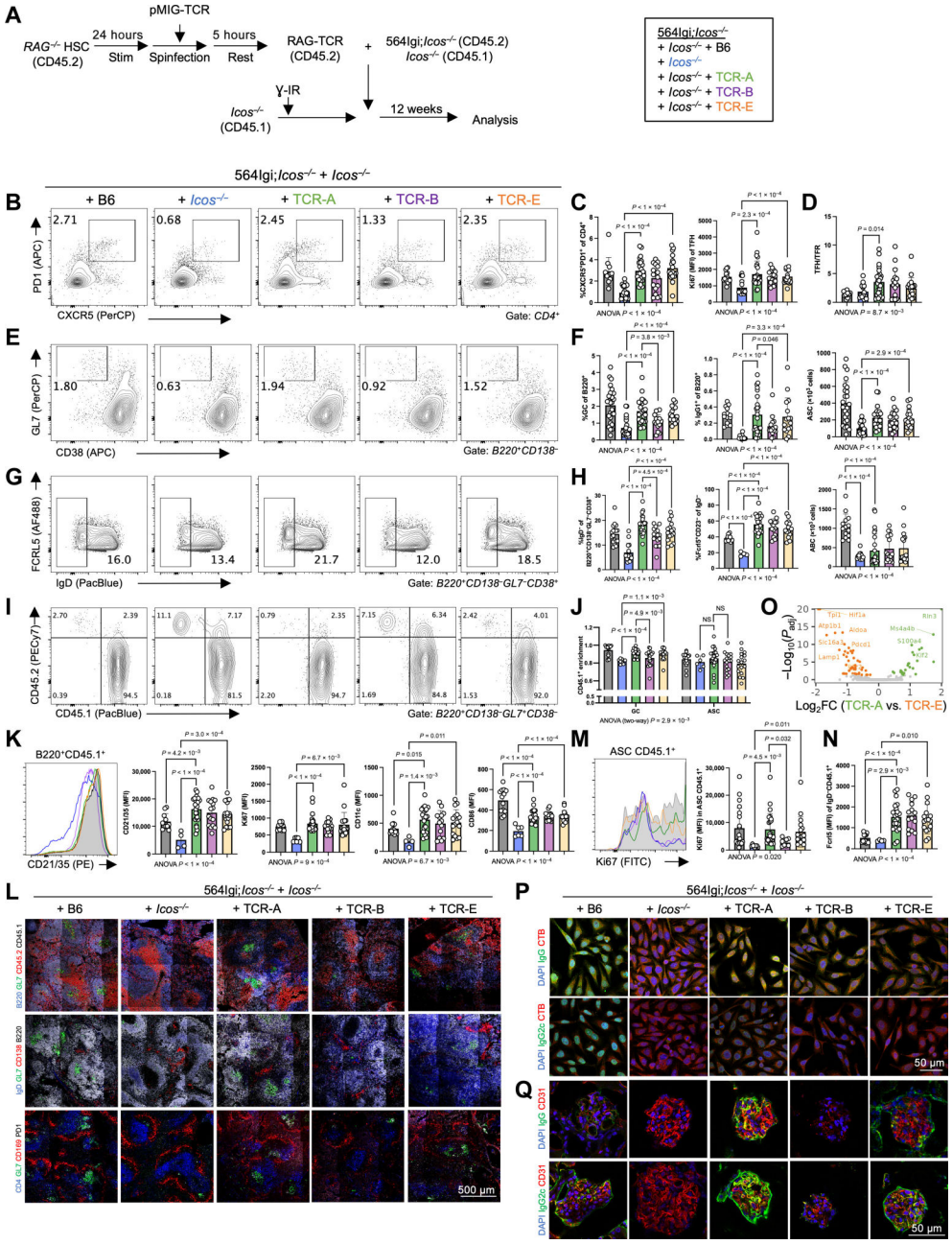

Fig. 6. A single autoreactive TFR clone is sufficient to initiate autoreactive GCs.

(**A**) Experimental diagram. Retrogenic donor stem cells were produced by spinfection of *RAG*$^{-/-}$ HSCs with retrovirus expressing TCR-A, TCR-B, or TCR-E and GFP (pMIG-TCR). *Icos*$^{-/-}$ (CD45.1) mice were lethally irradiated with 11 Gy, followed by intravenous reconstitution with a mix of 1p 564Igi;*Icos*$^{-/-}$ (CD45.2), 1p *Icos*$^{-/-}$ (CD45.1), and 1p B6, *Icos*$^{-/-}$, or retrogenic (CD45.2) HSCs. Twelve weeks after irradiation, mixed bone marrow chimeras were analyzed by flow cytometry. (**B** and **C**) Flow cytometry contour plots (B) and quantification (C) of follicular T cell frequency in the spleens of B6 (n = 11), *Icos*$^{-/-}$ (n = 23), TCR-A (n = 25), TCR-B (n = 17), and TCR-E (n = 18) mixed autoimmune chimeras. (**D**) Bar plot of the ratio of T_{Fh}

($CD4^+CXCR5^+PD1^+FoxP3^-$) to T_{FR} ($CD4^+CXCR5^+PD1^+FoxP3^+$) cells in the spleens of B6, *Icos*$^{-/-}$, TCR-A, TCR-B, and TCR-E mixed autoimmune chimeras. (**E** and **F**) Flow cytometry contour plots (E) and quantification (F) of Gc, $IgG1^+$ B cell frequency, and ASc ($CD138^+$) number in the spleens of B6, *Icos*$^{-/-}$, TCR-A, TCR-B, and TCR-E mixed autoimmune chimeras. (**G** and **H**) Flow cytometry contour plots (G) and quantification (H) of $IgD^-B220^+CD138^-GL7^-CD38^+$ B cells, $Fcrl5^+CD23^-B220^+CD138^-GL7^-CD38^+$ memory B cells, and ABCs ($CD11c^+CD21/35^-B220^+$ $CD138^-GL7^-CD38^+IgD^-$) in the spleens of B6, *Icos*$^{-/-}$, TCR-A, TCR-B, and TCR-E mixed autoimmune chimeras. (**I** and **J**) Flow cytometry contour plots (i) and quantification (J) of non-564Igi–derived ($CD45.1^+CD45.2^-$) GC, ASC, or ABC in the spleens of B6, *Icos*$^{-/-}$, TCR-A, TCR-B, and tcR-e mixed autoimmune chimeras. enrichment represents $cD45.1^+$ $cD45.2^-$ in indicated population relative to $cD45.1^+$ $cD45.2^-$ frequency in follicular B cells. (**K**) Flow cytometry histogram (left) and quantification (right) of cD21/35, Ki67, cD11c, and cD86 expression in non-564Igi–derived ($cD45.1^+cD45.2^-$) B cells in the spleens of B6, *Icos*$^{-/-}$, TCR-A, TCR-B, and TCR-E mixed autoimmune chimeras. (**L**) confocal microscopy of spleens from B6 ($n = 11$), *Icos*$^{-/-}$ ($n = 10$), TCR-A ($n = 4$), TCR-B ($n = 4$), and TCR-E ($n = 4$) mixed autoimmune chimeras stained for indicated markers. (**M**) Flow cytometry histogram (left) and quantification (right) of Ki67 in non-564Igi–derived ($CD45.1^+CD45.2^-$) ASCs in the spleens of B6, *Icos*$^{-/-}$, TCR-A, TCR-B, and TCR-e mixed autoimmune chimeras. (**N**) Bar plot of Fcrl5 expression in non-564Igi–derived ($CD45.1^+CD45.2^-$) $IgD^-B220^+CD138^-GL7^-CD38^+$ B cells in the spleens of B6, *Icos*$^{-/-}$, TCR-A, TCR-B, and TCR-E mixed autoimmune chimeras. (**O**) Volcano plot of differentially expressed genes between TCR-A (green) versus TCR-E (yellow) cells from scRNA-seq from Fig. 3A. Differential expression computed by MAST and adjusted for multiple comparison based on Bonferroni correction. (**P** and **Q**) Confocal microscopy of HEp-2 cells stained with sera (P) or kidneys (Q) from B6 ($n = 4$), *Icos*$^{-/-}$ ($n = 4$), TCR-A ($n = 4$), TCR-B ($n = 4$), and TCR-E ($n = 4$) mixed autoimmune chimeras stained for indicated markers. Data are representative of four independent experiments. Data are represented as means ± SD. *P* value computed using two-tailed Student's *t* test for two-way comparisons or ANOVA for grouped comparisons.

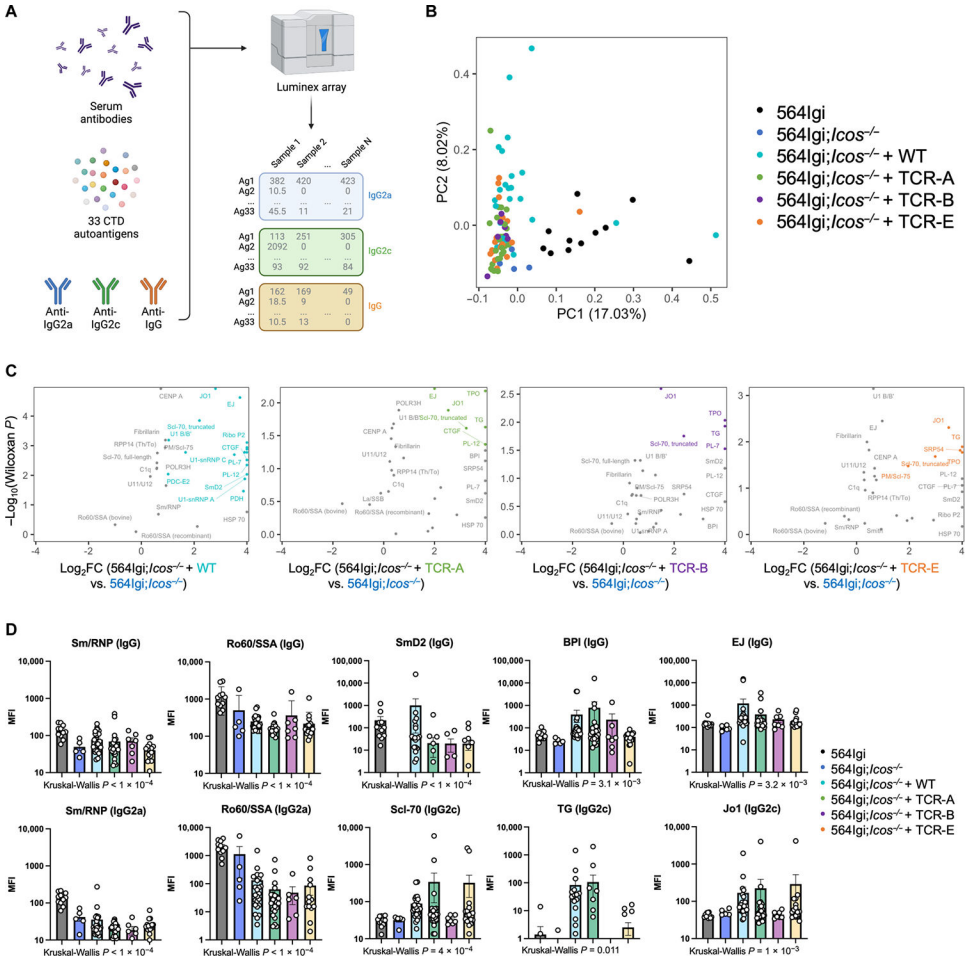

Fig. 7. TCR autoreactivity shapes B cell tolerance and epitope spreading.

(**A**) Experimental diagram. Serum autoreactivity was screened against 33 connective tissue disease (CTD) autoantigens by Luminex bead array. Antibody isotype subclasses were distinguished by secondary antibody staining. Created with BioRender.com. (**B**) Principal components analysis of serum reactivity from 564Igi ($n = 11$) or 564Igi;$Icos^{-/-}$ ($n = 5$) mice, or B6 ($n = 14$), TCR-A ($n = 24$), TCR-B ($n = 7$), or TCR-E ($n = 18$) mixed autoimmune chimeras. Component weightings were computed using MFI of all autoantigens and antibody subclasses for each sample. (**C**) Volcano plots of differential autoreactivity between sera from autoimmune chimeras versus 564Igi;$Icos^{-/-}$ mice. Fold change was computed using MFI of IgG binding, and P value was computed using Wilcoxon rank sum test. (**D**) Bar plots of serum reactivity for indicated autoantigen and antibody subclass. Data are represented as means ± SD.